NOTICE

CERTAIN DATA CONTAINED IN THIS DOCUMENT MAY BE DIFFICULT TO READ IN MICROFICHE PRODUCTS.

Conf-931118--1

ASTM Second Symposium on Constraint Effects in Fracture

AUTHOR'S NAMES:

T. J. Theiss[1], B. R. Bass[2], & J. W. Bryson[1]

TITLE OF PAPER: *

Experimental and Analytical Comparison of Constraint Effects Due To Biaxial Loading and Shallow-Flaws

AUTHOR'S AFFILIATIONS

[1]Development engineer, Oak Ridge National Laboratory, P. O. Box 2009, Oak Ridge, TN 37831-8056

[2]Senior Researcher, Oak Ridge National Laboratory, P. O. Box 2009, Oak Ridge, TN 37831-8056

---

* Research sponsored by the Office of Nuclear Regulatory Research, U.S. Nuclear Regulatory Commission under Interagency Agreement 1886-8011-9B with the U.S. Department of Energy under Contract DE-AC05-84OR21400 with Martin Marietta Energy Systems, Inc.

ABSTRACT: A program to develop and evaluate fracture methodologies for the assessment of crack-tip constraint effects on fracture toughness of reactor pressure vessel (RPV) steels has been initiated in the Heavy-Section Steel Technology (HSST) Program. The focus of studies described herein is on the evaluation of a micromechanical scaling model based on critical stressed volumes for quantifying crack-tip constraint through applications to experimental data. Data were utilized from single-edge notch bend (SENB) specimens and HSST-developed cruciform beam specimens that were tested in HSST shallow-crack and biaxial testing programs. Shallow-crack effects and far-field tensile out-of-plane biaxial loading have been identified as constraint issues that influence both fracture toughness and the extent of the toughness scatter band.

Results from applications indicate that the micromechanical scaling model can be used successfully to interpret experimental data from the shallow- and deep-crack SENB specimen tests. When applied to the uniaxially and biaxially loaded cruciform specimens, the two methodologies showed some promising features, but also raised several questions concerning the interpretation of constraint conditions in the specimen based on near-tip stress fields. Crack-tip constraint analyses of the shallow-crack cruciform specimen subjected to uniaxial or biaxial loading conditions are shown to represent a significant challenge for these methodologies. Unresolved issues identified from these analyses require resolution as part of a validation process for biaxial loading applications.

Introduction

Crack-tip constraint is an issue that significantly impacts fracture mechanics technologies employed in safety assessment procedures for the commercially licensed nuclear reactor pressure vessel (RPV). A validated technology that incorporates constraint effects is essential to the transfer of fracture toughness data from, for example, miniature fracture toughness surveillance specimens to RPVs. This capability could have a substantial impact on the outcome of probabilistic pressurized-thermal-shock (PTS) analyses and assessments of startup/cooldown transients of aging nuclear plants. This paper provides interim results from a program to evaluate selected fracture methodologies for the quantitative assessment of crack-tip constraint effects on fracture toughness of RPV steels.

Far-field tensile out-of-plane biaxial loading [1], and shallow-crack effects [2] have been identified as constraint issues that influence both fracture toughness and the extent of the fracture toughness scatter band. Relevance of these issues to RPV safety assessments is supported by several observations. First, PTS loading produces biaxial stress fields in an RPV wall that have no counterpart in conventional laboratory specimens used to generate fracture toughness data. Limited data indicate that a decrease in toughness is associated with biaxial loading [1]. Second, the probability of RPV vessel failure in PTS analyses is dominated by initiations from shallow cracks [3-5]. Recent testing has demonstrated an effective increase in fracture toughness of shallow cracks compared to deep-cracked specimens [2]. Determining the extent of the interaction between this toughness elevation associated with shallow cracks and toughness reduction due to biaxial loading effects is one of the main goals of the Heavy-Section Steel Technology (HSST) biaxial testing program [1].

The focus of the studies performed to date has been on evaluations of stress-based fracture methodologies (i.e., the J-Q model of O'Dowd and Shih [6-9] and the Dodds-Anderson constraint correction model [9-11]) through applications to experimental and fractographic data. These methodologies were selected for the initial evaluations because of their previously demonstrated promise as practical means for incorporating effects of crack-tip constraint into fracture assessments. Data for these assessments were obtained primarily from the HSST shallow-crack [2] and biaxial testing programs [1]. Shallow- and deep-crack single-edge notch bend (SENB) specimens and uniaxially and biaxially loaded cruciform specimens from these testing programs were analyzed using both the J-Q methodology and the Dodds-Anderson (D-A) fracture toughness constraint scaling model.

This paper is a summary of recent HSST investigations comparing experimental and fractographic data from the SENB shallow-crack and biaxial cruciform testing programs to the near-tip constraint analysis of those tests. Emphasis is given in this paper to the application of the Dodds-Anderson (D-A) fracture toughness scaling model to the SENB and cruciform experimental data. Additional information on the D-A scaling model and results of the application of the J-Q methodology to the test data and the comparison of the analytical results to the fractographic data are covered in Ref. 12. For completeness, this paper includes a summary of the shallow-crack and biaxial testing programs which have been reported previously [1, 2]. The finite-element analysis of the cruciform specimens used in the biaxial testing program in included in a following section. The next section in the paper outlines an overview of the J-Q methodology but details of the J-Q method applied to the test data is in Ref. 12. The results of the application of the D-A fracture toughness scaling model to the shallow-crack and cruciform test data comprises the next section. A discussion of crack-tip analysis which is applicable to both the J-Q method and the D-A scaling model is presented followed by a summary of the interim conclusions of this investigation.

Summary of Shallow-Crack Testing Program

1. Thirty-eight relatively large (W ~ 100 mm deep) laboratory beam specimens were tested to compare the behavior of specimens with shallow flaws to that of specimens with deep flaws.

2. The results showed conclusively that shallow-flaw beam specimens of A 533 B material have a significant increase in crack-tip-opening displacement (CTOD) or J_c toughness (~150%) and K_{Jc} toughness (~60%) over deep-crack specimens in the transition region of the toughness curve. All specimens were 100 mm deep (W). Shallow-crack beams had crack depths (a) ranging from 9 to 14 mm (a/W ~ 0.1 to 0.14), while deep-crack beams had 50-mm-deep cracks (a/W ~ 0.5).

3. There is little or no difference in toughness between deep- and shallow-flaw specimens on the lower shelf where linear-elastic conditions exist.

4. Varying the beam thickness from 50 to 150 mm had little or no influence on the toughness in both the shallow- and deep-crack specimens in spite of the fact that the American Society for Testing and Materials (ASTM) E-399 requirement for valid plane strain results were not met. This observation suggests that plane strain behavior for steels of this strength level differ from ASTM E399.

5. In the transition region of the fracture toughness curve, the increase in shallow-flaw toughness compared with deep-flaw toughness appears to be well characterized by a temperature shift of about 35°C. This temperature shift, which is crack-depth dependent, could be greater for shallower cracks that are also important in RPV safety assessments.

6. The two-parameter J-Q analysis methodology was used as a means of quantifying the effect of flaw depth on constraint and fracture toughness. Analysis results appear to support the utility of the J-Q concept and interpretation method to characterize the crack-tip fields up to the onset of crack initiation in specimens with either deep or shallow flaws. At J-critical (onset of cleavage initiation) for the deep-flawed specimens, the Q-stress was about zero, indicating small-scale yielding (SSY) conditions. At J-critical for the shallow-flawed specimens, the Q-stress was about −0.7. This negative Q-stress indicates a significant loss of constraint.

Biaxial Testing Program

Cruciform Bend Specimen

The configuration of the cruciform bend specimen used in the testing program is depicted in Fig. 1. The specimen has a cruciform-shaped geometry with a cross section with dimensions of 91 × 102 mm and a straight through-crack of uniform depth of 10 mm in the test section. The total length of this specimen in the longitudinal or transverse direction, including the test section and the loading arms, is 610 mm. Three slots are machined into each arm to minimize diffusion of the load around the test section containing the through-crack. The crack is cut between two opposite central load diffusion control slots to produce a two-dimensional (2-D) shallow crack with no singularity on the surface. Figure 1(*b*) shows the profile of the crack and the intersection of the crack and the central slot.

Instrumentation is placed on the specimen to monitor crack-mouth-opening displacement (CMOD), load-line displacement (LLD), surface strain, and temperature at various locations. A special load reaction system has been constructed for applying bending loads (P) to the arms of the specimen in a statically determinant manner. Loading is applied at midspan to the specimen using a square, flat seat having rounded edges and the same planar dimensions as the center test section. The test section bends into two orthogonal surfaces that contact the seat along the outer edges, resulting in eight-point bending (or four-point bending for the uniaxial case).

Test Matrix

The HSST Program assigned five cruciform specimens to the initial development phase of the biaxial testing program. These "development" specimens were used to evaluate the performance of the test specimen, test fixture, and procedures and to develop a test specimen geometry suitable for the generation of biaxial fracture toughness data.

Of the five development specimens, four were tested under biaxial loading, and one was tested under uniaxial loading. All biaxially loaded cruciform specimens were tested with a transverse-to-longitudinal load ratio of 0.6:1, as described in Ref. 1. The uniaxially loaded cruciform specimen allows comparison with previous uniaxial SENB shallow-crack specimens under identical test conditions (crack depth, temperature, etc.). Testing cruciform specimens in both uniaxial and biaxial loading configurations will allow toughness values to be measured with only one test condition changed, namely, the out-of-plane loading.

Test conditions were selected to facilitate comparison of data from the cruciform specimens with previous HSST shallow-crack data tested under uniaxial conditions [2]. Several of the uniaxial shallow-crack tests were conducted at $T - RT_{NDT} = -10°C$, which is in the transition region of the deep-crack toughness curve for A 533 B steel. The A 533 B steel used for the test section material in these tests has an RT_{NDT} of $-35°C$. Therefore the test temperature for the cruciform specimen tests was set at $-45°C$. The cruciform specimens were 91 mm deep with a crack depth of 10 mm. The beam width and crack depth of the cruciform specimen are approximately the same as for the HSST shallow-crack beams.

Experimental Results and Interpretation

Of the five specimens tested, one biaxial test (designated BB-3) initiated at the intersection of the crack tip and the load diffusion control slot. This result is questionable since the stress concentration at the slot could have influenced the failure load. As a result, this test was not interpreted in terms of toughness. Additional details are included in Ref. 1. The interpretable test results indicate that the critical load for each specimen was similar but that in the uniaxial test (BB-2) the specimen was able to withstand substantially more (≈60%) deflection (LLD or CMOD) than the biaxial tests (BB-1, -4, and -5). (Strains imposed in these tests were substantially higher than any that would be produced in an RPV either from normal or accident loading; this is a consequence of testing in the transition region of the toughness curve.) In addition, the plastic "work" at the crack tip as defined by either the plastic area under the P-LLD

curve or the P-CMOD curve (defined as U_{pl} or A_{pl}, respectively) in the three biaxial tests was about one-third of the corresponding uniaxial value of U_{pl} or A_{pl}. Furthermore, the critical displacements (LLD or CMOD) and work performed (U_{pl} or A_{pl}) were consistent for the three interpretable biaxial test results. These results indicate a pronounced reduction in the ductility of the material at fracture (as measured by critical displacement or work) due to biaxial loading.

Toughness data for the biaxial and uniaxial cruciform specimens were calculated using the techniques described in Ref. 1. The critical J-integral values were converted to critical elastic-plastic, stress-intensity factors K_{Jc} using the plane strain formulation. The data necessary to estimate J and the resulting toughness values are tabulated in Ref. 1. The P vs CMOD method is considered the more sensitive of the techniques examined for determining fracture toughness shallow-flaw specimens and is the primary method used for the cruciform specimen analysis.

Toughness results for the SENB and cruciform specimens expressed in terms of K_{Jc} are shown in Figs. 2–4 (taken from Ref. 1). Figure 2 shows the deep- and shallow-crack uniaxial toughness data as a function of normalized temperature. The data at $T - RT_{NDT} = -10°C$ are plotted as a function of crack depth in Fig. 3 and as a function of load ratio in Fig. 4. Examination of the data in Figs. 2–4 reveals several important points. First, biaxial loading appears to reduce the fracture toughness compared with either the uniaxial cruciform value from test BB-2 or the SENB data. The average of the biaxial toughness is ≈20% less than the uniaxial cruciform value and ≈18% less than the average of the uniaxial SENB and cruciform results. Second, the uniaxial cruciform value is consistent with the SENB toughness results; this tends to validate the use of the cruciform specimen for uniaxial data generation. Third, the scatter band of the biaxial data may be less than that associated with the uniaxial, shallow-crack data. An increase in toughness and scatter is associated with loss of constraint in laboratory specimens. Results presented in Fig. 3 indicate that biaxially loaded cruciform specimens yield results with reduced scatter. The trends in the biaxial and uniaxial cruciform data described here are tentative results based on very limited data. Additional data are required to substantiate these trends and to provide better quantification of the effect of biaxial loading on fracture toughness. Nonetheless these initial results strongly suggest that an improved understanding of the shallow-flaw and biaxial loading effects would significantly impact the fracture mechanics technologies employed in reactor safety assessments.

Finite-Element Analysis of Cruciform Specimen

Three-dimensional elastic-plastic, finite-element analyses were performed on the cruciform specimen depicted in Fig. 1. Local crack-tip stress fields obtained from these analyses are used in applications of stress-based constraint characterization models. The one-fourth section of the cruciform specimen is represented in the 3-D finite-element model of Fig. 5. The model consists of 18,650 nodes and 3,890 twenty-node isoparametric brick elements. Collapsed-prism elements arranged in a focused or centered fan configuration at the crack tip are used to produce a 1/r strain singularity appropriate for inelastic analysis. Reduced integration was employed to eliminate shear locking in the elements. The cruciform specimen is assumed to be supported on a rigid plate under the test section [i.e., the area defined by (-51 mm $\le z \le 0$, $0 \le x \le 51$ mm) in Fig. 5] and loaded by uniformly applied forces at the ends of the longitudinal/transverse arms (i.e., locations C and D in Fig. 5) to produce the uniaxial or biaxial bending conditions. The rigid support plate is incorporated into the finite-element model of Fig. 5 using a contact element option in the ABAQUS (Ref. 13) finite-element program.

The full geometry of the load-diffusion control slots is represented in the finite-element model [Fig. 5(*b*)]. The slot geometry incorporated in the model is represented by the configuration of Fig. 6(*d*), which was used for test specimens BB-4 and -5. The same finite-element model was used for analysis of specimen BB-2, although the latter employed a different slot configuration [Fig. 6(*c*)]. The model also incorporated a highly refined mesh in the crack-tip region [Fig. 5(*c*)] to provide resolution of stress fields over the normalized distance $2 \le r\sigma_0/J \le 5$ in front of the crack.

The outermost semicircular ring of nodes in the mesh of Fig. 5(*c*) has a radius of 2 mm. This radius was extended to 4 mm in a second finite-element model developed for analysis of the BB-2 test [Fig. 5(*d*)]. The relatively higher failure load (measured in terms of J) of the latter test required an expanded region of refinement to resolve the stress at a normalized distance ahead of the crack tip of $r\sigma_0/J = 5$.

The material properties used for all calculations presented herein include Young's modulus E = 205,170 MPa, Poisson's ratio $\nu = 0.25$, and the piecewise linear stress-strain curve. The stress-strain curve represents a modification of material data for A 533 grade B class 1 steel taken from Ref. 14. The modification consists of an adjustment of the yield stress to produce better agreement with load vs CMOD data from the biaxial tests (described below).

Results from small-strain analyses of tests BB-2 (uniaxially loaded specimen) and BB-4 and -5 (biaxially loaded specimens) are compared with measured data in Figs. 7 and 8. Because geometry and test conditions were essentially the same for BB-4 and -5, only one computation was performed for the biaxial loading case. In Fig. 7, the calculated longitudinal load vs LLD curves (measured at point C in Fig. 5) are compared with measured data from each of the three tests (BB-2, -4, and -5). Comparisons of calculated and measured longitudinal load vs CMOD for the same tests are given in Fig. 8. Both Figs. 7 and 8 show good agreement between the computed and measured load vs deflection curves for the BB-2 test. Minor differences between the CMOD curves in Fig. 8 for BB-2 may be partly due to differences in the slot configurations in the model and in the BB-2 test specimen. The load vs deflection curves for specimens BB-4 and -5 are within the data scatter for the two tests.

Stress Triaxiality (J-Q) Method

One of the methods used to assess the effects of shallow-crack depths and biaxial loading on crack-tip stress triaxiality is the J-Q methodology. The J-Q method was applied to the shallow- and deep-crack SENB specimens previously [2].The J-Q method applied to the uniaxial and biaxial cruciform specimen is based on analyses described in the previous section. Results of the J-Q analyses from both test series are presented in Ref. 12. Additional results of the crack-tip analysis interpreted in terms of the Q-stress are presented later section in this paper. The J-Q methodology is summarized here for completeness.

The definition of Q-stress employed here is given by O'Dowd and Shih [8] in the form

$$Q(\tilde{r}) = \frac{\sigma_{\theta\theta}(\tilde{r}) - \sigma_{\theta\theta}(\tilde{r})\big|_{SSY}}{\sigma_0} \qquad (1)$$

where $\tilde{r} = r/(J/\sigma_0)$ is a normalized distance measured in the crack plane ahead of the crack tip ($\theta = 0$); the r, θ polar coordinate system is centered at the crack tip such that $\theta = 0$ corresponds to the crack plane ahead of the tip. In Eq. (1), the Q-stress measures the departure of the opening-mode stress $\sigma_{\theta\theta}$ from the reference plane strain SSY solution, normalized by the yield stress σ_0.

Using a modified boundary layer (MBL) formulation, O'Dowd and Shih [8] determined that the Q-stress characterizes the magnitude of a spatially uniform (approximately) hydrostatic stress state in a forward sector ($|\theta| \le \pi/2$ and $1 \le \tilde{r} \le 5$) of the crack-tip region. The Q-stress, although

found to be essentially independent of $\tilde{r}$, was formally defined at $\tilde{r} = 2$, which falls just outside the finite strain blunting zone. For conditions ahead of the crack that do not conform to a spatially uniform hydrostatic stress field, O'Dowd and Shih [8] introduced Eq. (1) to emphasize the explicit dependence of Q upon distance $\tilde{r}$. The latter definition of Q-stress is convenient for applications presented in Ref. 12 due to the spatial dependence of Q determined for certain loading conditions applied to the cruciform specimen.

Fracture Toughness Scaling Model (Dodds-Anderson)

The Dodds-Anderson (or D-A) scaling model [11] analyzes constraint conditions by determining the area (or volume when considering a 3-D geometry) within a particular stress contour for a finite-body geometry and scaling that area (or volume) with an equivalent SSY solution. The SSY state is then considered to yield true fracture toughness results completely independent of specimen size or loading and is comparable to a specimen of infinite size. The scaling model has been successfully applied to fracture toughness results exhibiting either a loss of in-plane constraint (i.e., shallow cracks) or out-of-plane constraint (i.e., thickness effects) [11]. The scaling model assumes that the volume of critically stressed material surrounding the crack tip is the same in different specimens with different constraint conditions. As a result, the SSY critical fracture toughness can be determined in a high-constraint geometry and then applied to a low-constraint geometry or vice versa.

Application of Scaling Model to Shallow-Crack Data

The D-A scaling model has been used to investigate both in-plane and out-of-plane constraint loss in the HSST shallow- and deep-crack test results. The in-plane investigation is reported herein; the application of the model to out-of-plane constraint or thickness effects is the subject of a separate report [15]. The scaling model was applied to the shallow-crack data using information available in the literature [16] without the need of additional crack-tip analysis.

The fracture toughness data from the HSST shallow-crack program are shown in Fig. 9 as a function of normalized temperature ($T - RT_{NDT}$). The shallow-crack toughness increase can be quantified by a temperature shift of ~35°C. The data within the box at a normalized temperature range of approximately –10°C to –25°C in Fig. 9 are replotted in Fig. 10 as a function of crack depth. As expected in a low-constraint geometry, Fig. 10 shows both an increase in the fracture toughness values and data scatter from the shallow-crack specimens when compared with the

deep-crack specimens. The regression analysis shown in Fig. 10 indicates a mean shallow-crack toughness value of about 1.6 times the deep-crack toughness as previously reported [2].

Using the D-A [10] analysis results, Wallin [16] has quantified in-plane constraint loss by the following equation:

$$J_{FB}/J_0 = 1 + 176\,(J_{FB}/a\sigma_0)^{1.37}\ , \qquad (2)$$

where J_0 is the SSY or reference value of J, and J_{FB} is the value of J in the finite body geometry. Equation (2) is applicable to materials with a Ramberg–Osgood hardening exponent of ~10, such as A 533 B steel. It is recommended in Ref. 11 that results from the above equation not be used in situations in which $J/J_0 > 4$. The SSY value (J_0) was computed from Eq. (2) for each specimen tested as a part of the HSST shallow-crack program. The plane-strain elastic modulus was used to convert from J to K.

The K_0 values as a function of crack depth in the transition region are shown in Fig. 11. The data in Fig. 11 correspond to the uncorrected data in Fig. 10. As indicated in Fig. 11, the K_0 results are reduced to a toughness level independent of the crack depth of the specimens. Comparing Figs. 10 and 11, the deep-crack data in Fig. 11 experience little to no reduction to their K_0 values, while the shallow-crack data are reduced substantially to almost exactly the same toughness level. The regression analysis shown in Fig. 11 confirms that the K_0 data are independent of crack depth. The mean and standard deviation of the shallow- and deep-crack data are included on Fig. 11 as well. The mean values are almost identical at 112 MPa$\sqrt{m}$ for the shallow-crack K_0 data and 114 MPa$\sqrt{m}$ for the deep-crack K_0 data. The shallow-crack K_0 also exhibit substantially less scatter than the original shallow-crack data in Fig. 10. The standard deviation of the original shallow-crack K_{Jc} data was 37.2 MPa$\sqrt{m}$; the shallow-crack K_0 data had a deviation of only 8.1 MPa$\sqrt{m}$. All of the data in Fig. 11 met the criteria of $J_{FB}/J_0 \le 4$ except one specimen that had a J_{FB}/J_0 ratio of ~5.6. The average J_{FB}/J_0 ratio for the shallow-crack specimens in Fig. 11 was 2.73; the average deep-crack specimen J_{FB}/J_0 value was 1.05.

Several conclusions can be drawn from the application of the D-A scaling model to the HSST shallow-crack data. First, the scaling model works very well with the shallow-crack data. The model adjusts both shallow- and deep-crack data to the SSY toughness value. In addition, the scatter in the corrected toughness data was also reduced by the application of the scaling model to the original shallow-crack toughness results. Furthermore, the scaling model is very simple to use in this application. The analysis of the data using the scaling model required no additional crack-tip analysis. The constraint corrections were based on specimen geometry and cleavage

toughness results. It appears likely that J_c predictions for shallow-crack geometries could be made from K_o data obtained from deep-crack specimens.

Application of Scaling Model to Cruciform Beam Data

Dodds et al. [9] have also developed a methodology for performing constraint adjustments of fracture toughness data from test specimens that utilize a J-Q description of the crack-tip stress fields. This methodology has the advantage of being computationally simpler to apply than the stressed-volume technique for constraint correction previously introduced by Dodds and Anderson [11]. Applications of this simplified approach to data from the uniaxially and biaxially loaded cruciform specimens, which draw upon the J-Q analyses of the previous section, are presented herein.

The modified D-A scaling procedure, like the scaling model previously described, determines the ratio of finite-body toughness to SSY toughness (i.e., J_{FB}/J_o). The modified D-A scaling procedure is based on the observation [9] that even under different constraint conditions the shape of the principal stress contour ahead of the crack tip remains the same, with only the size varying. This relationship is maintained until deformation becomes excessive. Critically stressed areas ahead of the crack can be related to critical distances ahead of the crack, which allows the use of the near-tip stress field to determine J_{FB}/J_o. Figure 12 shows the stresses ahead of the crack tip for the SSY solution and the cruciform specimen under uniaxial and biaxial loading. The uniaxial and biaxial stresses are at (or near) the critical value of J. This allows the determination of the constraint conditions (and J_o toughness) in these specimens at failure (i.e., critical SSY toughness, J_o). The three biaxial specimens yielded toughness values sufficiently close such that only one J value for these specimens is necessary.

Two different methods of applying the D-A scaling procedure were used for these results. Both methods begin with the ratio of the distance ahead of the crack tip, $\tilde{r}$, for the finite-body and SSY solutions to determine the J_{FB}/J_o ratio. Both methods begin the construction with an $\tilde{r}$ value of about 2. The first method holds the finite-body stress constant at $\tilde{r} = 2$ and determines the distance ahead of the crack tip in the SSY solution that corresponds to that stress (see Fig. 12). The second method begins with the SSY stress at $\tilde{r} = 2$ and finds the distance corresponding to that stress in the finite-body solution(s). Both of these methods are outlined in Fig. 12. The first method begins with the finite-body stress at $\tilde{r} = 2$ or $r = 2J_{FB}/\sigma_o$. The distance in the SSY solution that yields the same critical stress is $\tilde{r} = 11.63$ or $r = 11.63\ J_o/\sigma_o$. Because the critical

distances are assumed equal, J_{FB}/J_o = 11.63/2.0 or 5.82. The second method yields a J_{FB}/J_o of 2.0/0.621 = 3.22.

The two methods of applying the D-A scaling model just described yield J_{FB}/J_o ratios that are quite different. Theoretically, as discussed in Ref. 9, both methods should yield identical results. One reason for this problem is that these are numerical approximations to the stresses near the crack tip, which always contain some error. The SSY stress solution tends to flatten as distance from the crack tip increases, which could exaggerate the error in J_{FB}/J_o with increasing distance from the crack tip. Furthermore, the first D-A scaling method used distances greater than $\tilde{r}$ = 10, which is typically far beyond the process zone for cleavage fracture. (Additional information on the location of the cleavage origin site ahead of the crack tip are presented in Ref. 12.) For the two reasons just outlined, the second D-A scaling procedure that uses smaller distances ahead of the crack tip is the preferred method in this investigation and will be used to interpret the results.

The J_{FB}/J_o results using the D-A scaling procedure for the uniaxial and biaxial cruciform specimens at $\tilde{r}$ = 1.5 to 4 are plotted as a function of distance ahead of the crack tip in Fig. 13. Examination of these results leads to several observations. First, the J ratios (and subsequently J_o) vary as a function of distance ahead of the crack tip. For the uniaxial cruciform, the J_{FB}/J_o ratio increases from ~3 at $\tilde{r}$ = 1.5 to ~4 at $\tilde{r}$ = 4. The biaxial cruciform shows a similar increase in J_{FB}/J_o with distance ahead of the crack tip. In Ref. 9, the calculation of J_o is considered valid when values determined at $\tilde{r}$ = 1.5 and at $\tilde{r}$ = 4 differ by <10%. The variation in J_{FB}/J_o (and subsequently J_o) shown in Fig. 13 is about 25% over this range for both the uniaxial and biaxial cases. The D-A scaling model results do not, therefore, meet the criteria established in Ref. 9.

There are two potential explanations for J_o varying by more than the accepted criteria of 10%. The first is the nature of the cruciform specimen itself, which possesses 3-D stress fields that vary through the thickness. The D-A scaling model allows the use of critically stressed areas ahead of the crack, assuming a relatively constant field through a specimen thickness. The second explanation is the assumption that the stressed areas in these cases are similarly shaped, allowing the comparison of distances ahead of the crack rather than areas. This assumption could lead to variations in J_o that might not exist had the D-A scaling model used contour areas.

Figure 13 indicates that the range of J_{FB}/J_o ratios for the uniaxial cruciform is consistent with previous J_{FB}/J_o values for the shallow-crack SENB specimens. The uniaxial cruciform yields values of J_{FB}/J_o between 3 and 4; the shallow-crack SENB specimens yielded J_{FB}/J_o ratios ranging from 1.8 to 5.6, averaging ~2.7. Finally, as shown in Fig. 13, the biaxial J_{FB}/J_o ratio is

~25% greater than the uniaxial J-ratio. This implies greater constraint loss for the biaxial specimen than the uniaxial specimen, a result which is inconsistent with the experimental toughness results. However, these ratios have been determined for a very limited number of tests. Additional tests will be necessary to determine if these trends continue.

The K_o values were calculated for the uniaxial and biaxial cruciform tests for comparison with SENB K_o values using the analytically based J_{FB} values and the J_{FB}/J_o ratios determined at $\tilde{r} = 2$ and the plane-strain conversion from J to K. The ratio at $\tilde{r} = 2$ was chosen because the Q-stress is typically determined at that location and the biaxial and uniaxial stresses ahead of the crack tip are almost identical at that location (see Fig. 12). The K_o values for the four cruciform tests are shown in Fig. 11 along with the upper and lower SSY toughness (K_o) results from the shallow- and deep-crack SENB tests. As indicated in Fig. 11, all of the cruciform SSY toughness values are within the range of SSY data from the SENB specimens. The K_o values from the biaxial cruciform are near the lower limit of the SENB K_o range; the uniaxial K_o value was nearer the upper limit. Additional data are necessary to determine the full range of SSY toughness values under uniaxial and biaxial loading.

Discussion of Crack-Tip Analyses

The J-Q method and D-A scaling model have been applied to the shallow- and deep-crack SENB tests and the uniaxial and biaxial cruciform tests. Data sets used in these applications are generated from tests of specimen geometries that provide a contrast in analytical modeling requirements. The SENB specimen is modeled in terms of a 2-D plane strain formulation, while the cruciform specimen exhibits a fully 3-D character that must be considered. Analysis results indicate that both methodologies can be used successfully to interpret experimental results from the deep- and shallow-crack SENB specimen tests. Applications of the two methodologies to the cruciform specimen each showed promising features, but they also raised several issues concerning constraint analysis based on near-tip stress fields. These issues have been identified and discussed in the preceding sections. Some additional observations of the limitations of the two methods applied to the cruciform specimen are presented herein.

Figure 12 shows the stresses ahead of the crack tip for the SSY solution and the uniaxial and biaxial cruciform specimens at the critical value of J. Because both the J-Q method and the scaling model are based on the stresses ahead of the crack tip, observations about Fig. 12 are germane to both techniques. First, the coincidence of the critical crack-tip stresses near the crack tip ($\tilde{r} \leq 2$) is encouraging and indicates the potential applicability of these methods to the

uniaxial and biaxial cruciform specimens. Furthermore, both the uniaxial and biaxial stresses deviate significantly from the SSY solution, indicating that the J-integral alone cannot characterize the crack-tip stresses. The crack-tip stresses for the uniaxial and biaxial cruciform specimens begin to diverge at $\tilde{r} = 2$, which reflects that the far-field bending stresses are beginning to impinge on the crack-tip stresses in the uniaxial case. In other words, at distances very near the crack tip, ($\tilde{r} \leq 2$), the stresses are dominated by the crack-tip singularity. At distances satisfying $\tilde{r} > 2$, however, the stresses tend to be influenced by the far-field bending stress, resulting in a divergence of the uniaxial and biaxial stresses. Physically, $\tilde{r} \geq 2$ represents a distance ahead of the crack tip of 1.2 and 0.8 mm for the uniaxial and biaxial cruciform specimens, respectively. These distances are well within the corresponding plastic zone radius that is conservatively estimated, from the plane strain relation [17] to be 14 and 9.6 mm for the uniaxial and biaxial case at failure, respectively. In reality, both the uniaxial and biaxial specimens have reached a condition of uncontained yielding at the point of failure.

The difference between the SSY stresses and the uniaxial and biaxial stresses (i.e., the Q-stress) ahead of the crack tip is shown in Fig. 14. The Q-stress for the uniaxial specimen is not constant within the range of $\tilde{r} = 1.5$ to 5 because of the interaction of the bending stresses with the crack-tip singular stresses. In fact, the uniaxial stresses in Fig. 12 between $\tilde{r} = 6$ and 8 appear to be controlled by the far-field bending stress, resulting in a near linear stress distribution. If the identical load were applied to the specimen in a tensile manner rather than through bending loads, the Q-stress for the uniaxial specimen is expected to be more uniform than shown in Fig. 14. It is anticipated, however, that the bending stress field will influence the uniaxial and biaxial specimens less as the specimen size increases and/or the load at failure decreases.

In contrast with the uniaxial specimen, the biaxial Q-stress shown in Fig. 14 is relatively constant over the distances shown. In fact, the biaxial Q-stress at failure agrees well with the shallow-crack Q-stress determined from the SENB specimens. The reason for the constant biaxial Q-stress appears to be due to offsetting effects. First, the bending stress tends to drive the Q-stress more negative with distance from the crack tip as in the uniaxial case. The offsetting effect is the out-of-plane biaxial load itself. The addition of the out-of-plane stress increases the hydrostatic stress, which in turn increases the opening-mode stress. The offsetting nature of the bending stress and the out-of-plane stress cannot be generalized, however, for other biaxially loaded specimens.

The application of crack-tip analysis to a shallow-crack cruciform specimen under biaxial loading such as described in this chapter represents a significant challenge for these techniques.

Differences in constraint conditions due to a biaxial load are difficult to quantify because of the absence of an appropriate distance parameter. Out-of-plane constraint (i.e., thickness effects) can be quantified in terms of the specimen thickness B. In-plane constraint loss is similarly related to a shallow-crack depth, a or a/W. Biaxial loading, however, which impacts the crack-tip stresses substantially, has no appropriate length scale or distance parameter to which the constraint condition can be related. Another way of considering the influence of biaxial loading is that the out-of-plane stress appears to make the specimen benave as a larger uniaxial specimen.

The final impact of out-of-plane biaxial loading is not fully known at this time. It is known, however, that biaxial loading does impact the conditions at the crack tip in a significant manner under conditions of uncontained yielding. Preliminary estimates from Ref. 18 indicated that under contained yielding, changes in initiation toughness due to biaxial effects would not exceed a few percent. Biaxial effects were exhibited in the cruciform specimen at conditions beyond contained yielding. The analyses confirm previously described experimental trends. As shown in Fig. 12, uniaxial and biaxial near-tip stresses ($\tilde{r} \leq 2$) are coincident at failure loads. The applied load at which failure occurred in the uniaxial and biaxial specimens is almost identical; however, the critical value of toughness (note J in the legend of Fig. 12) is quite different. Biaxial loading further alters the way that applied load on a cracked specimen is related to the crack-driving force. Biaxial loading also substantially reduces the ductility of a specimen. Additional crack-tip analysis and additional biaxial tests are necessary before the impact of the biaxial loads on the fracture resistance of an RPV is understood.

Summary and Conclusions

Applications of the D-A scaling model to data obtained from shallow- and deep-crack SENB specimens produced very good results. The scaling model provided adjusted SSY toughness values in the transition region that were virtually identical for deep- and shallow-crack data. In addition to removing the influence of crack depth in the toughness data, the scaling model reduced the scatter associated with the shallow-crack data.

When the scaling model was applied to the cruciform data, the results were again more difficult to interpret than the SENB application. In the original formulation of the scaling model, toughness data are adjusted to SSY values based on ratios of areas (or volumes) within stress contours around the crack tip. The engineering model applied to the cruciform specimens approximates these ratios from the stress distribution directly ahead of the crack tip. Stresses very close to the crack tip ($\tilde{r} < 2$) were used to determine the J_{FB}/J_0 ratios for the cruciform

specimens. These ratios were found to vary ~25% over the annulus $1.5 < \tilde{r} < 4$ for both uniaxial and biaxial load cases. This difference exceeds the maximum of 10% recommended in Ref. 11 for a valid calculation of J_o. Also, the biaxial J_{FB}/J_o ratio was ~25% greater than the uniaxial ratio, which implies a greater constraint loss for the biaxial specimen than the uniaxial specimen. The latter result is inconsistent with toughness results determined from experimental data. All of the cruciform SSY toughness values determined from these ratios, however, were within the range of SSY data from the SENB specimens.

Applications of the J-Q and D-A constraint methodologies presented herein utilized data sets generated from tests of specimen geometries that provide a contrast in analytical modeling requirements. The shallow- and deep-crack SENB specimen is modeled in terms of a 2-D plane-strain formulation, while the fully 3-D character of the uniaxially and biaxially loaded cruciform specimen must be considered. Analysis results from applications indicate that both methodologies can be used successfully to interpret experimental data from the shallow- and deep-crack SENB specimen tests. The two methodologies showed some promising features in applications to the cruciform specimen, but also raised a number of questions concerning the interpretation of constraint conditions in the specimen from near-tip stress fields. The more successful interpretations of these methodologies applied to the SENB data are partially explained by the greater number of available data points. Crack-tip constraint analyses of the shallow-crack cruciform specimen subjected to uniaxial or biaxial loading conditions represent a significant challenge for these methodologies. Unresolved issues identified from these analyses and summarized in the foregoing discussion require resolution as part of a validation process for biaxial loading applications. Additional cruciform specimens need to be tested before any conclusion can be reached concerning the application of these methods to the cruciform data.

Some additional observations concerning applications to the cruciform specimen are presented herein. The near-tip stresses ahead of the crack are the focal point of the stress-based fracture methodologies applied in this study. The uniaxial cruciform specimen exhibited a substantial interaction of the near-tip and far-field bending stresses, which provided a contrast to a relatively uniform hydrostatic (i.e., Q-stress) field ahead of the crack tip in the SENB specimen. The biaxial specimen appears to be influenced by offsetting effects that also result in a spatially independent Q-stress field ahead of the crack. The far-field stresses, which tend to lower the near-tip stresses, are almost exactly offset by the out-of-plane stress component that increases the opening-mode stress in the biaxial specimen. This offsetting effect, however, cannot be generalized to biaxial specimens having different dimensions or load ratios. In addition, the impact of the far-field bending stress on the near-tip stresses would be reduced in specimens

having larger dimensions. Testing of a limited number of larger biaxial cruciform specimens, such as currently planned within the HSST Program, would provide additional data to quantify these effects.

The primary problem with using techniques described herein to examine the influence of biaxial loading is the absence of an appropriate length scale with which to quantify constraint. Differences in out-of-plane constraint are quantified by the specimen thickness; in-plane constraint is related to crack depth, but biaxial loading cannot be related to a similar length parameter. Examination of analytical results from this study indicates that biaxial loading produces a near-tip stress pattern similar to that expected of a larger specimen under uniaxial loading (i.e., biaxial loading increases the "effective" size of the specimen). However, additional data and analyses are necessary to substantiate this observation.

References

1. T. J. Theiss et al., "Initial Results of the Influence of Biaxial Loading on Fracture Toughness," USNRC Report NUREG/CR-6036 (ORNL/TM-12349), June 1993.

2. T. J. Theiss, D. K. M. Shum, and S. T. Rolfe, "Experimental and Analytical Investigation of the Shallow-Flaw Effect to Reactor Pressure Vessels," USNRC Report NUREG/CR-5886 (ORNL/TM-12115), July 1992.

3. R. D. Cheverton and D. G. Ball, "Pressurized-Thermal-Shock Evaluation of the H. B. Robinson Nuclear Power Plant," pp. 263–306, USNRC Report NUREG/CR-4183 (ORNL/TM-95657/V1), September 1985.

4. R. D. Cheverton and D. G. Ball, "Pressurized-Thermal-Shock Evaluations of the Calvert Cliffs Nuclear Power Plant," pp. 201–244, USNRC Report NUREG/CR-4022 (ORNL/TM-9408), September 1985.

5. R. D. Cheverton and D. G. Ball, "Preliminary Development of an Integrated Approach to the Evaluation of Pressurized Thermal-Shock as Applied to the Oconee 1 Nuclear Power Plant," pp. 5.1–5.51, USNRC Report NUREG/CR-3770 (ORNL/TM-9176), May 1986.

6. N. P. O'Dowd and C. F. Shih, "Family of Crack-Tip Fields Characterized by a Triaxiality Parameter: Part I—Structure of Fields," *J. Mech. Phys. Solids* 39, 989–1015 (1991).

7. N. P. O'Dowd and C. F. Shih, "Family of Crack-Tip Fields Characterized by a Triaxiality Parameter: Part II—Fracture Applications," *J. Mech. Phys. Solids* 40, 939–963 (1992).

8. N. P. O'Dowd and C. F. Shih, "Two Parameter Fracture Mechanics: Theory and Applications," USNRC Report NUREG/CR-5958 (CDNSWC/SME-CR-16-92), February 1993.

9. R. H. Dodds, C. F. Shih, and T. L. Anderson, "Continuum and Micromechanics Treatment of Constraint in Fracture," Report UILU-ENG-92-2014, November 1992.

10. R. H. Dodds, T. L. Anderson, and M. T. Kirk, "A Framework to Correlate a/W Ratio Effects on Elastic-Plastic Fracture Toughness (J_c)," *Int. J. Frac.* 48, 1–22 (1991).

11. T. L. Anderson and R. H. Dodds, "Specimen Size Requirements for Fracture Toughness Testing in the Ductile-Brittle Transition Region," *J. Test. Eval.* 19, 123–134 (1991).

12. B. R. Bass, et. al., "Biaxial Loading and Shallow-Flaw Effects on Crack-Tip Constraint and Fracture Toughness," USNRC Report NUREG/CR-6132 (ORNL/TM-12498), to be published.

13. *ABAQUS Theory Manual*, Version 4-8, Hibbitt, Karlson, and Sorensen, Inc., Providence, R.I., 1989.

14. D. J. Naus et al., "High-Temperature Crack-Arrest Behavior in 152-mm-Thick SEN Wide Plates of Quenched and Tempered A 533 Grade B Class 1 Steel," USNRC Report NUREG/CR-5330 (ORNL/TM-11083), April 1989.

15. T. J. Theiss and S. K. Iskander, "Constraint and Statistical Analyses of Transition Range A533 B Toughness Data," USNRC Report NUREG/CR-6106 (ORNL/TM-12467), to be published.

16. K. Wallin, "Statistical Aspects of Constraint with Emphasis on Testing and Analysis of Laboratory Specimens in the Transition Region," pp. 264–288 in *Constraint Effects in Fracture, ASTM STP 1171*, E. M. Hackett, K. H. Schwalbe, and R. H. Dodds, Eds., American Society for Testing and Materials, 1993.

17. J. M. Barsom and S. T. Rolfe, *Fracture and Fatigue Control in Structures—Applications in Fracture Mechanics*, 2nd Ed., Prentice-Hall, Englewood Cliffs, New Jersey, 1987.

18. D. K. M. Shum et al., "Analytical Studies of Transverse Strain Effects on Fracture Toughness for Circumferentially Oriented Cracks," USNRC Report NUREG/CR-5592 (ORNL/TM-11581), April 1991.

List of Figures

ORNL-DWG 92M-3935AR ETD

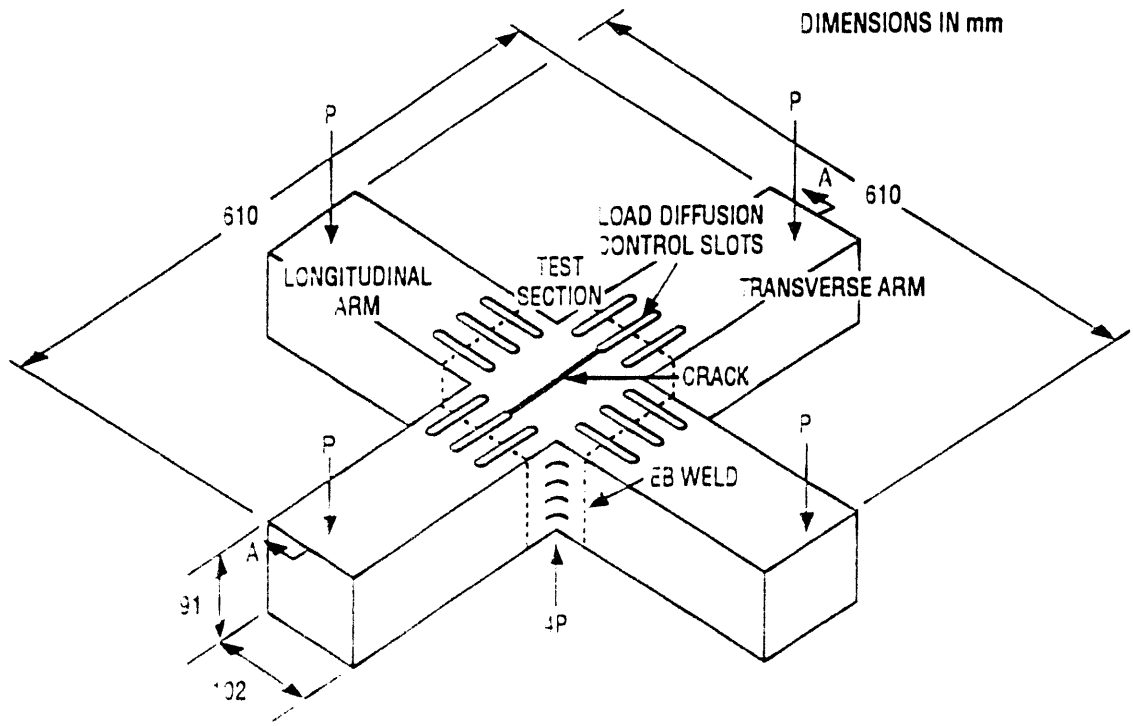

a)

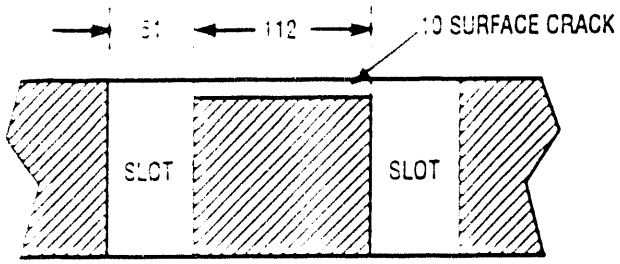

b) SECTION A-A

Fig. 1

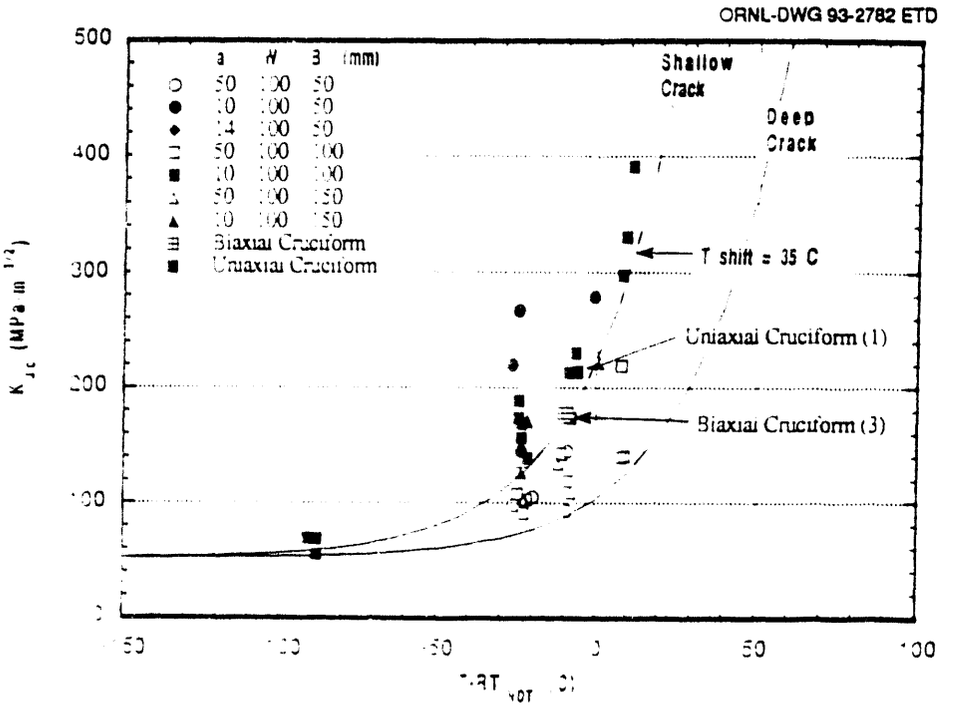
ORNL-DWG 93-2782 ETD
a W B (mm)
50 100 50
10 100 50
14 100 50
50 100 100
10 100 100
50 100 150
10 100 150
Biaxial Cruciform
Uniaxial Cruciform
Shallow Crack
Deep Crack
T shift = 35 C
Uniaxial Cruciform (1)
Biaxial Cruciform (3)
500
400
300
200
100
0
-150
-100
-50
0
50
100
K_{Jc} (MPa m$^{1/2}$)
T-RT$_{NDT}$ (C)

Fig. 2

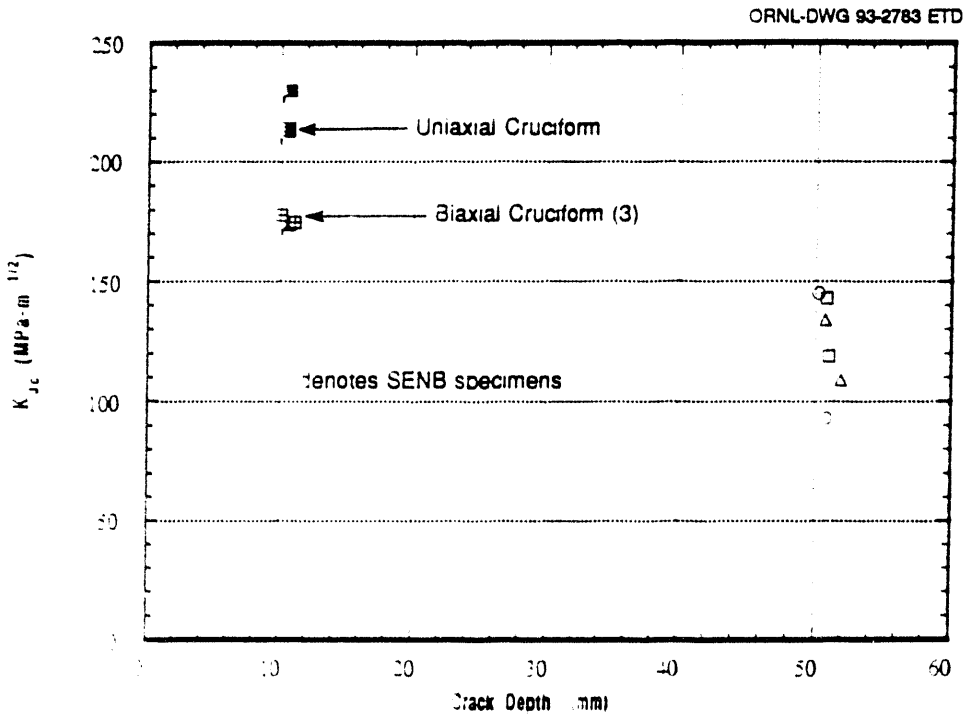
ORNL-DWG 93-2783 ETD
250
200
150
100
50
Uniaxial Cruciform
Biaxial Cruciform (3)
denotes SENB specimens
10
20
30
40
50
60
Crack Depth (mm)

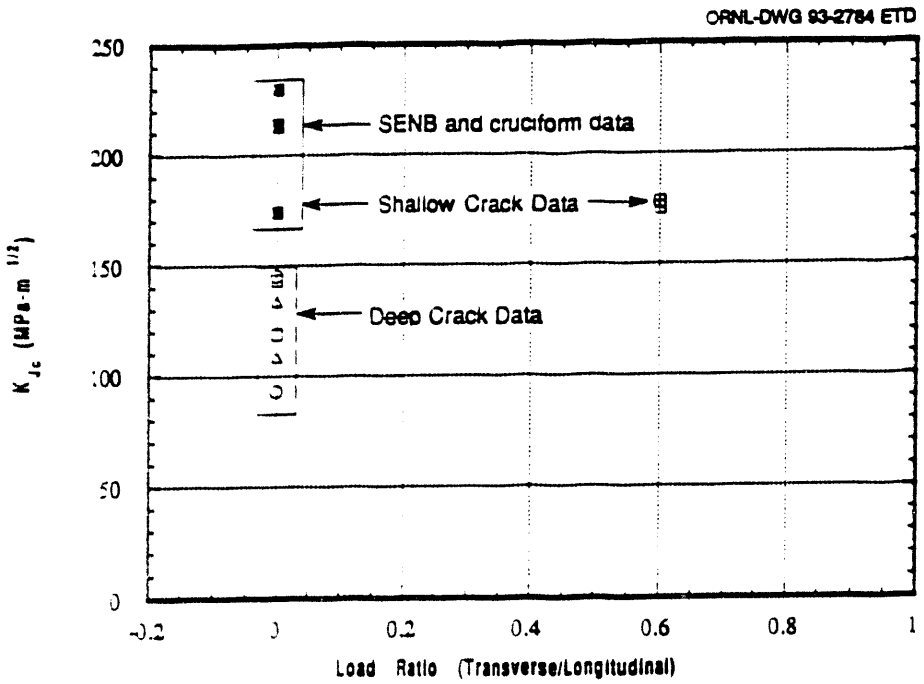
ORNL-DWG 93-2784 ETD
250
200
150
100
50
0
-0.2
0
0.2
0.4
0.6
0.8
1
SENB and cruciform data
Shallow Crack Data
Deep Crack Data
K_{Jc} (MPa·m$^{1/2}$)
Load Ratio (Transverse/Longitudinal)

Fig. 4

ORNL-DWG 93-3902 ETD

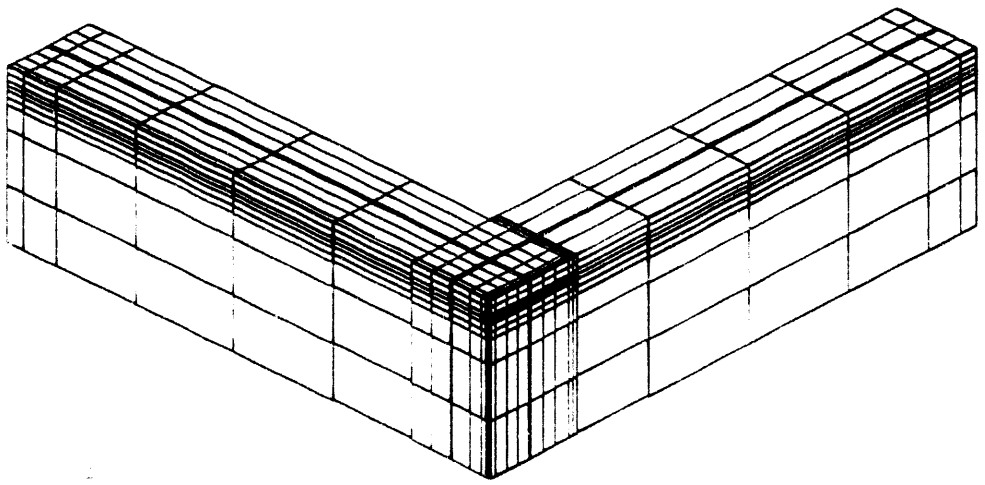

a)

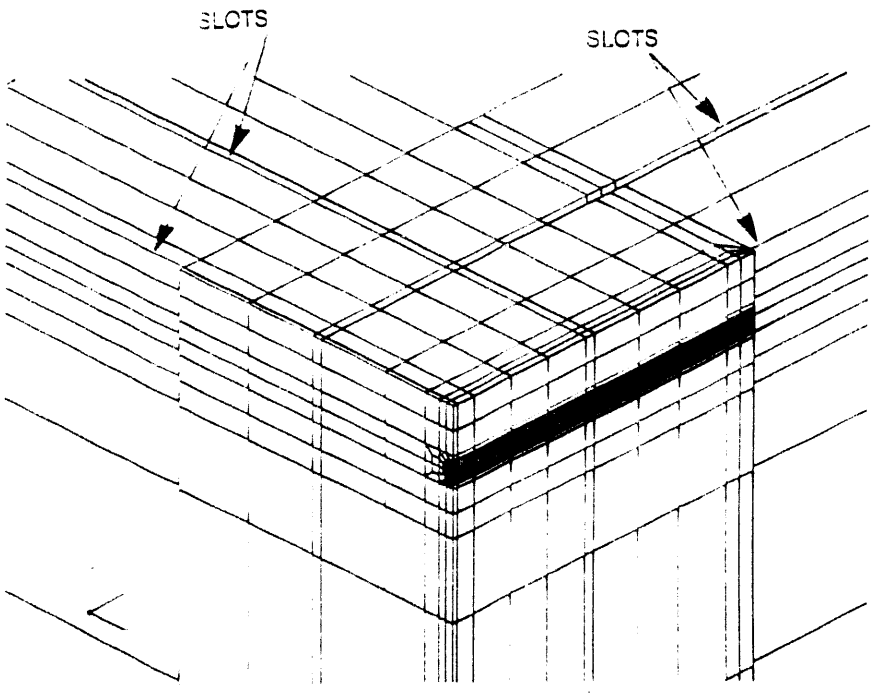

b)

Fig. 5

ORNL-DWG 93-3903 ETD

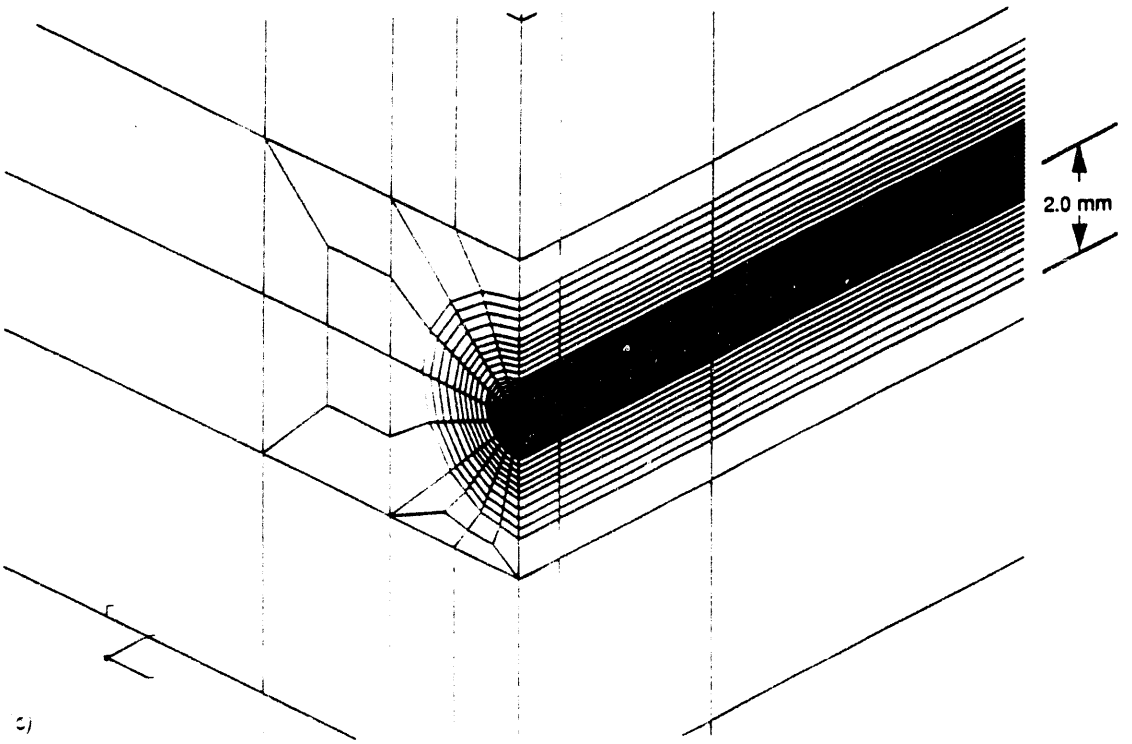

c)

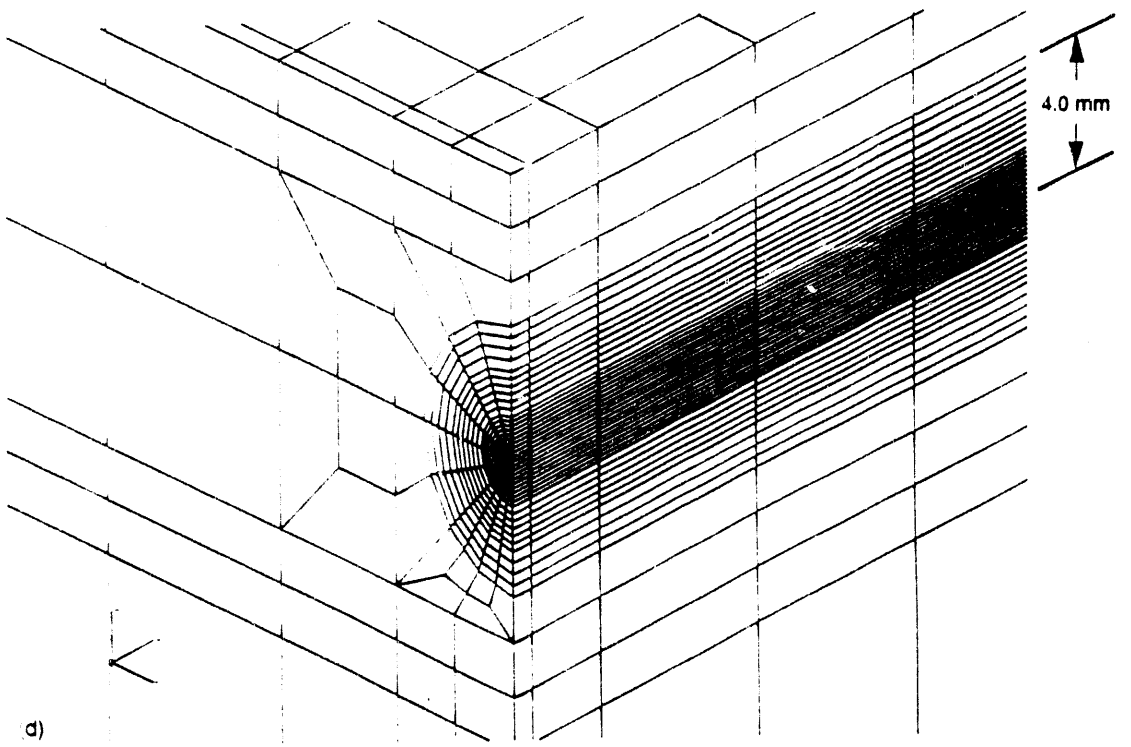

d)

ORNL-DWG 93-2729 ETD

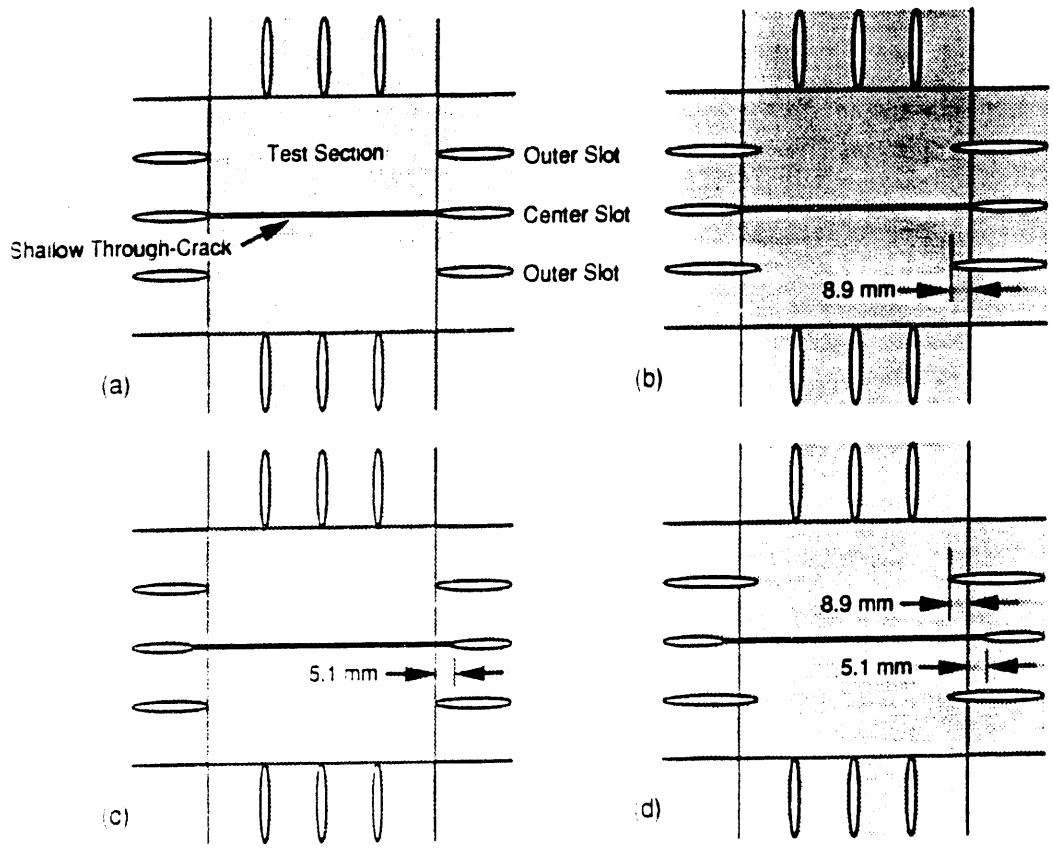

Fig. 6

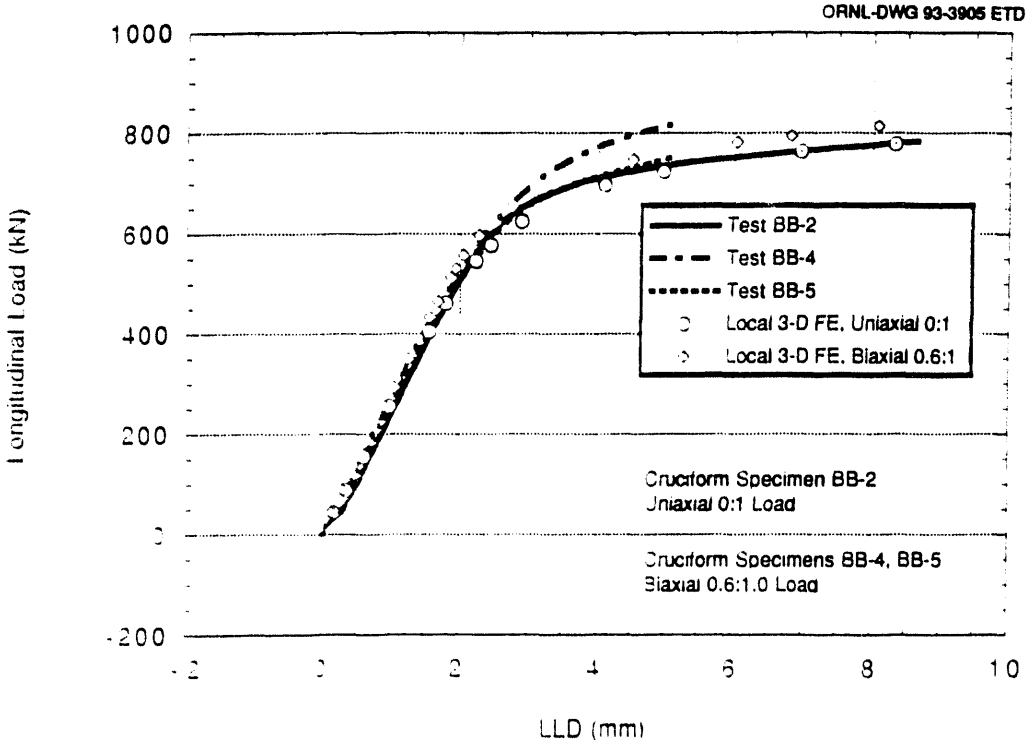
ORNL-DWG 93-3905 ETD
1000
800
600
400
200
0
-200
-2
0
2
4
6
8
10
Longitudinal Load (kN)
LLD (mm)
Test BB-2
Test BB-4
Test BB-5
Local 3-D FE, Uniaxial 0:1
Local 3-D FE, Biaxial 0.6:1
Cruciform Specimen BB-2
Uniaxial 0:1 Load
Cruciform Specimens BB-4, BB-5
Biaxial 0.6:1.0 Load

Fig. 7

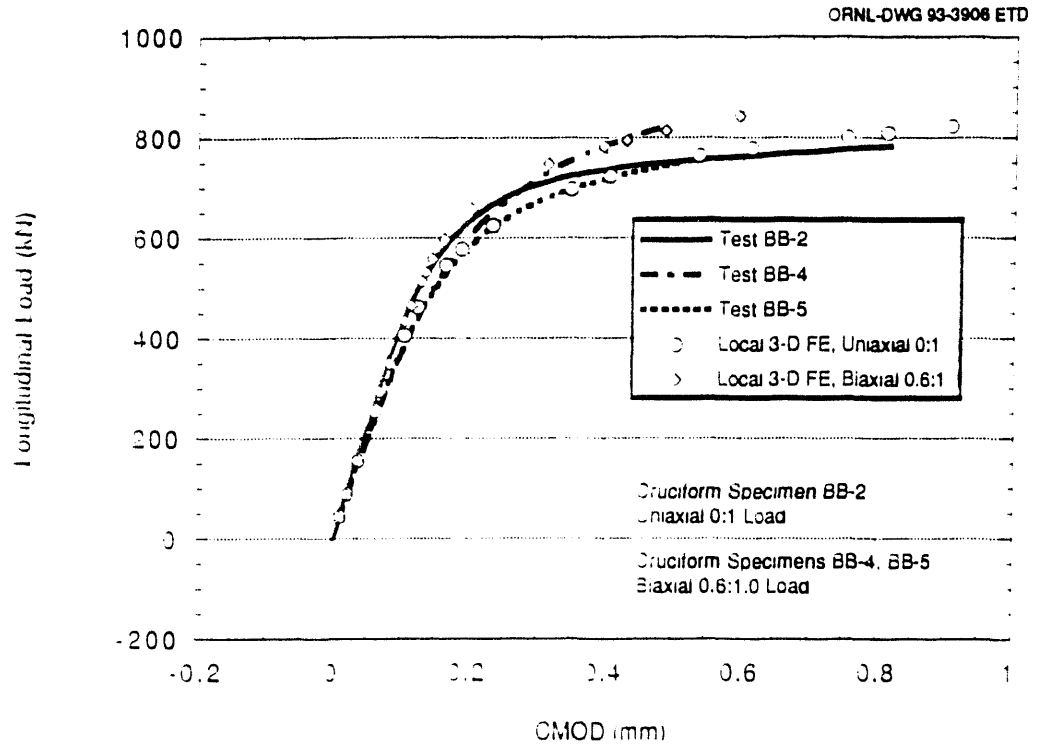
ORNL-DWG 93-3906 ETD
1000
800
600
400
200
0
-200
-0.2
0
0.2
0.4
0.6
0.8
1
Longitudinal Load (kN)
CMOD (mm)
Test BB-2
Test BB-4
Test BB-5
Local 3-D FE, Uniaxial 0:1
Local 3-D FE, Biaxial 0.6:1
Cruciform Specimen BB-2
Uniaxial 0:1 Load
Cruciform Specimens BB-4, BB-5
Biaxial 0.6:1.0 Load

Fig. 3

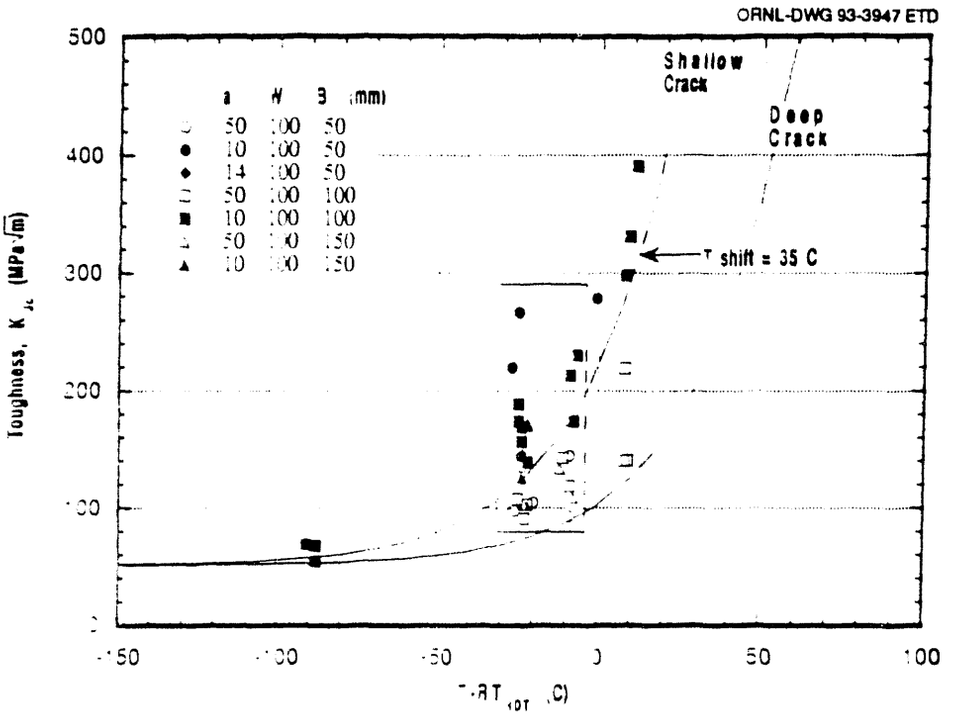
ORNL-DWG 93-3947 ETD
Shallow Crack
Deep Crack
a W B (mm)
50 100 50
10 100 50
14 100 50
50 100 100
10 100 100
50 100 150
10 100 150
T shift = 35 C
Toughness, K
500
400
300
200
100
0
-150
-100
-50
0
50
100
T-RT
(C)

Fig. 9

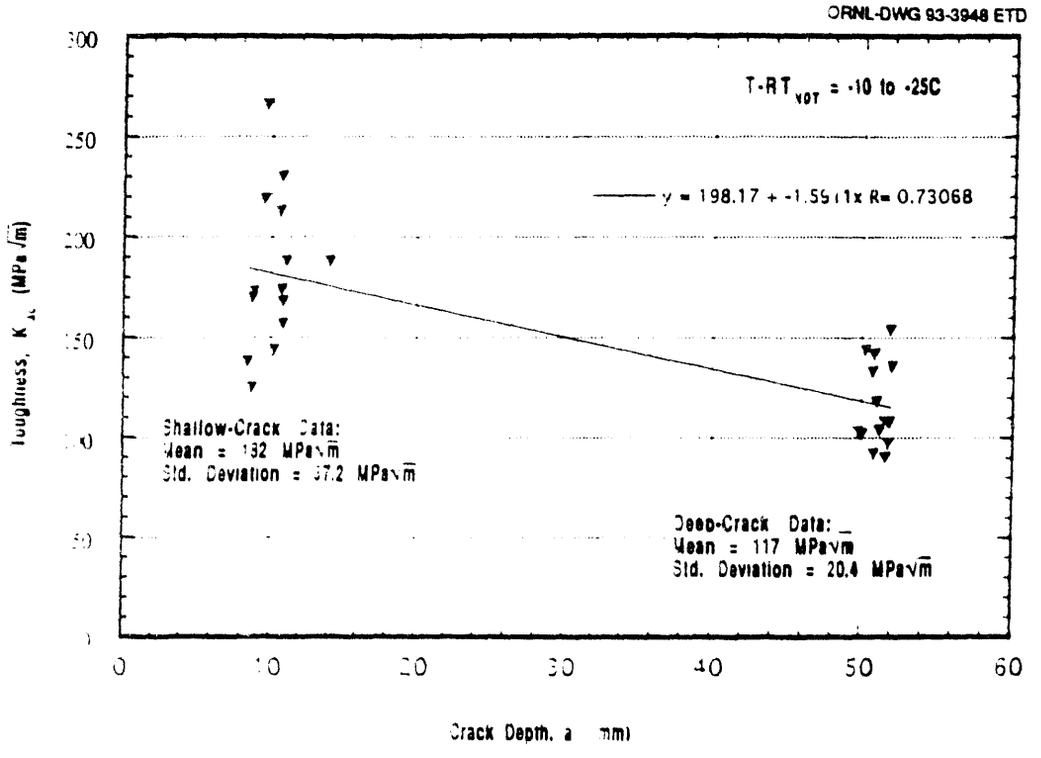
ORNL-DWG 93-3948 ETD
T-RT$_{NDT}$ = -10 to -25C
y = 198.17 + -1.59(1x R= 0.73068
Shallow-Crack Data:
Mean = 132 MPa√m
Std. Deviation = 37.2 MPa√m
Deep-Crack Data: _
Mean = 117 MPa√m
Std. Deviation = 20.4 MPa√m
Toughness, K$_{Jc}$ (MPa √m)
Crack Depth, a (mm)
0
10
20
30
40
50
60
250
200
150

Fig. 10

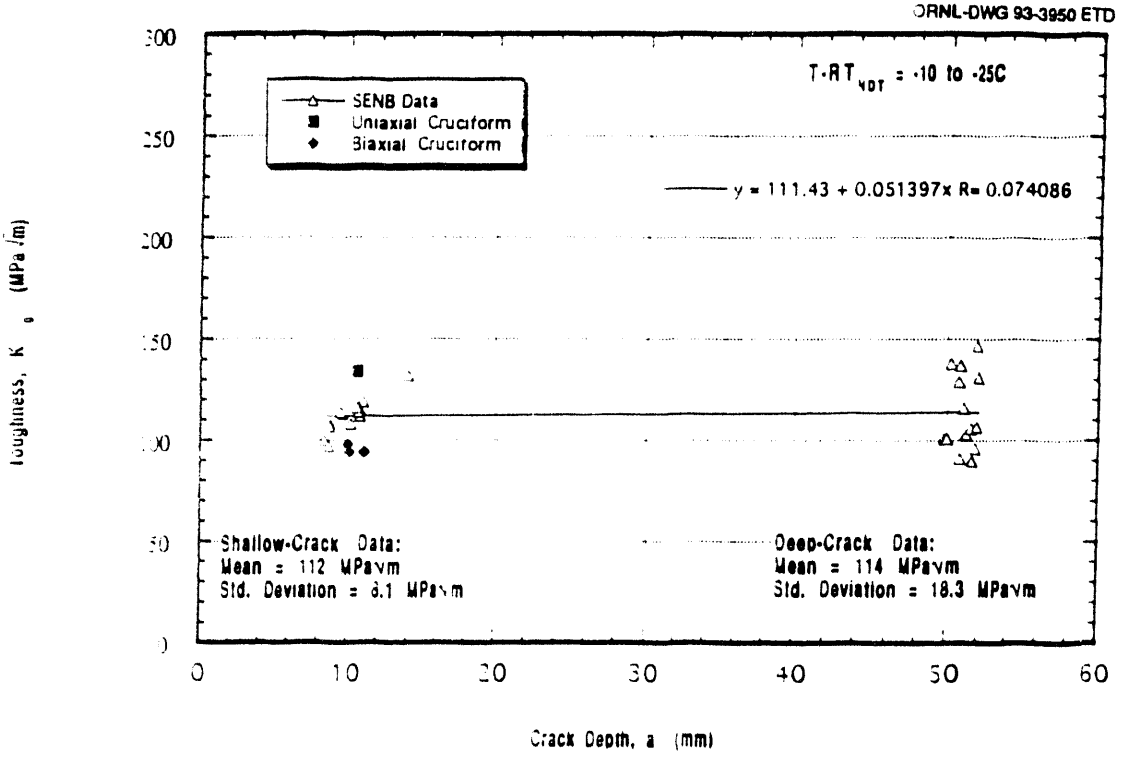
ORNL-DWG 93-3950 ETD
T-RT$_{NDT}$ = -10 to -25C
SENB Data
Uniaxial Cruciform
Biaxial Cruciform
y = 111.43 + 0.051397x R= 0.074086
Shallow-Crack Data:
Mean = 112 MPa√m
Std. Deviation = 8.1 MPa√m
Deep-Crack Data:
Mean = 114 MPa√m
Std. Deviation = 18.3 MPa√m
Toughness, K$_0$ (MPa√m)
Crack Depth, a (mm)
0
10
20
30
40
50
60

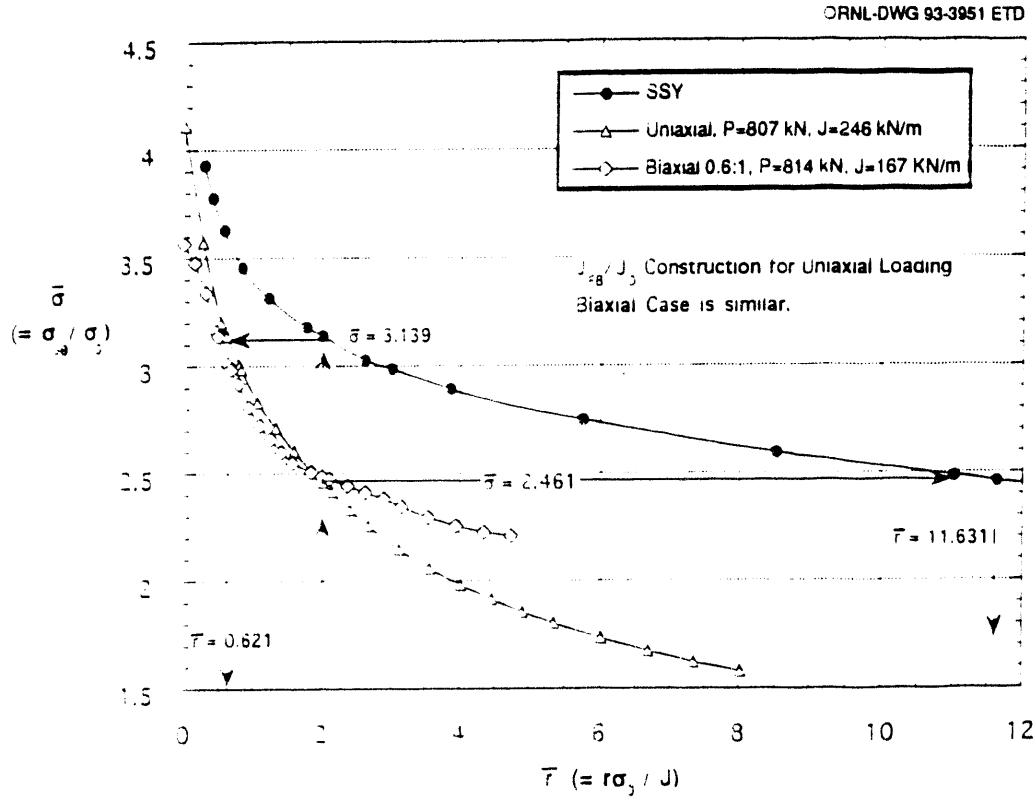
ORNL-DWG 93-3951 ETD
SSY
Uniaxial, P=807 kN, J=246 kN/m
Biaxial 0.6:1, P=814 kN, J=167 KN/m
J_{eB} / J_3 Construction for Uniaxial Loading
Biaxial Case is similar.
$\bar{\sigma}$ = 3.139
$\bar{\sigma}$ = 2.461
$\bar{r}$ = 11.6311
$\bar{r}$ = 0.621
$\bar{\sigma}$ (= σ_e / σ_3)
$\bar{r}$ (= rσ_3 / J)
4.5
4
3.5
3
2.5
2
1.5
0
2
4
6
8
10
12

Fig. 12

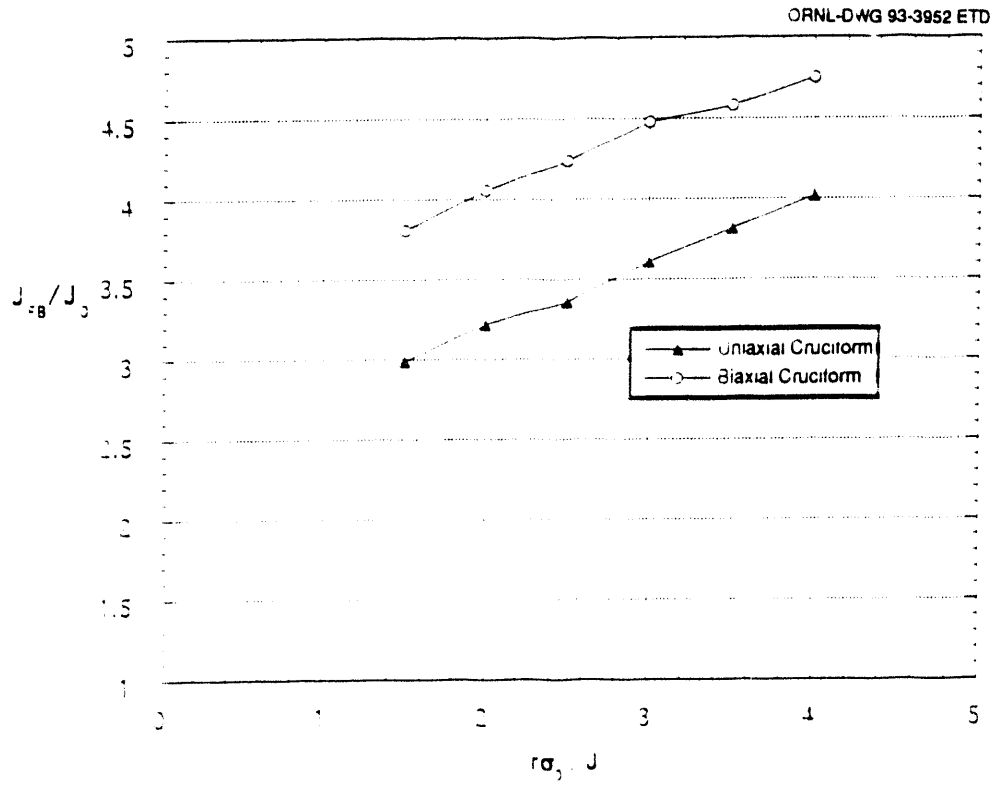
ORNL-DWG 93-3952 ETD
5
4.5
4
3.5
3
2.5
2
1.5
1
0
1
2
3
4
5
Uniaxial Cruciform
Biaxial Cruciform

-9

Fig. 12

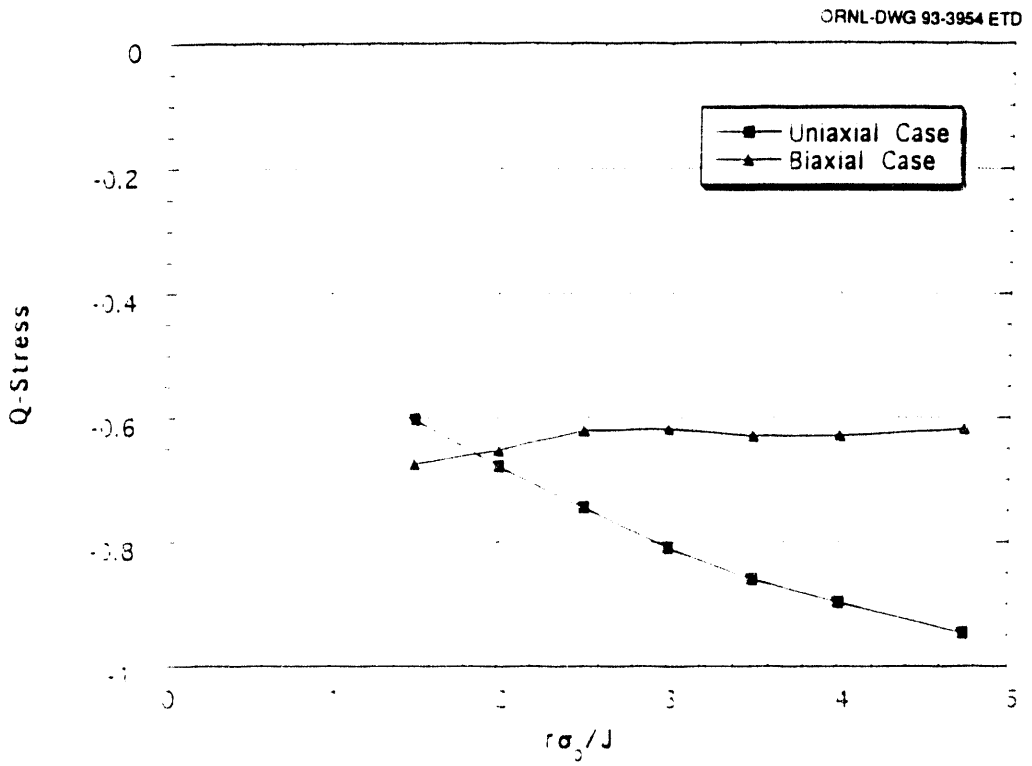
ORNL-DWG 93-3954 ETD
0
-0.2
-0.4
-0.6
-0.8
Q-Stress
Uniaxial Case
Biaxial Case
0
4
5
$r\sigma_y/J$

Fig. 14

EXPERIMENTAL AND ANALYTICAL COMPARISON OF CONSTRAINT EFFECTS DUE TO BIAXIAL LOADING AND SHALLOW FLAWS

T. J. Theiss, B. R. Bass, & J. W. Bryson
Heavy-Section Steel Technology Program (HSST)
Oak Ridge National Laboratory (ORNL)

2nd ASTM Symposium on Constraint Effects in Fracture
Ft. Worth, Texas

November 17-18, 1993

Research sponsored by the Office of Nuclear Regulatory Research, U.S. Nuclear Regulatory Commission under Inter-agency Agreement 1886-8011-9B with the U.S. Department of Energy under Contract DE-AC05-84OR21400 with Martin Marietta Energy Systems, Inc.

The HSST Program is Investigating Effects of Biaxial Loading Conditions and Shallow-Crack Geometries on Constraint Conditions and, Consequently, on Transfer of Toughness Data to RPVs

- Stress-based fracture characterizations
  - J-Q methodology of O'Dowd and Shih
  - Constraint correction technique of Dodds and Anderson

- Stress-strain-based characterizations, i.e. plane strain ductility techniques due to Clausing, Barsom, Merkle, and other researchers

- Alternative methodologies focusing on modified constitutive relations (eg. void-growth,strain-softening, etc)

Dual Parameter Fracture Correlations Provide a Measure of the Effect of Crack-Tip Constraint on Fracture Toughness

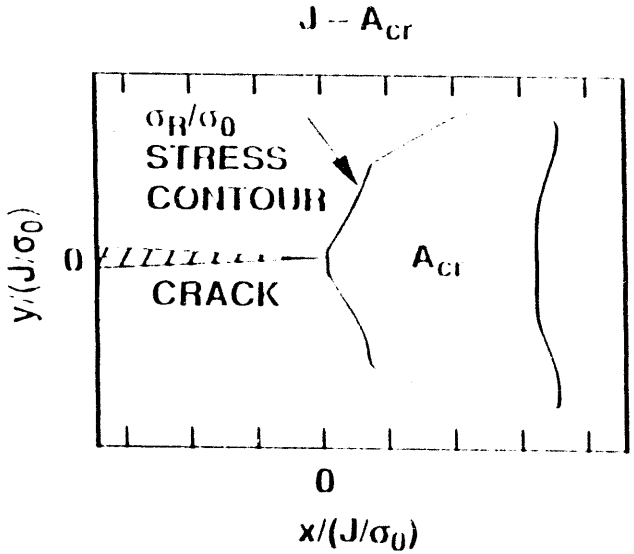

A_{cr} is the area over which stresses exceed the reference stress ratio (σ_R/σ_0) for crack initiation

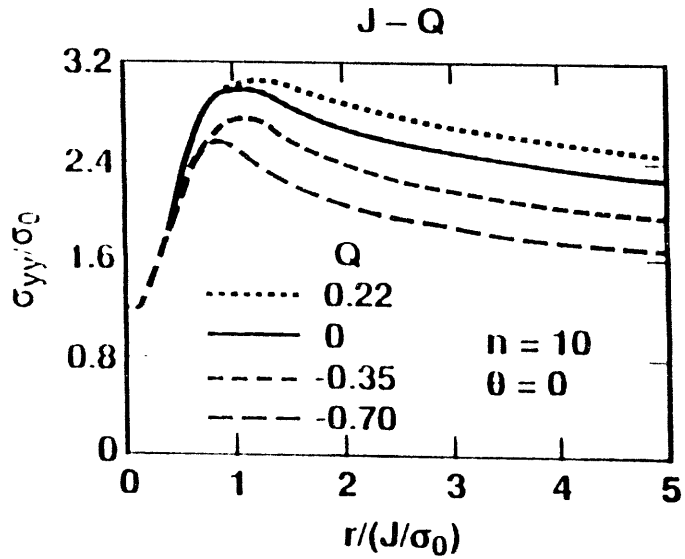

Q is a parameter characterizing the hydrostatic stresses and therefore the maximum principal stresses ahead of the crack

ORNL DWG 91M 3220R ETD

These methods are being applied to the shallow-crack and biaxial loading fracture toughness test data

Prototypical Flaw Depths Were Tested in the 100-mm-Deep Beams Used in the Shallow-Flaw Program

ORNL DWG 93M 3649 ETD

Shallow-Crack Fracture Toughness Data Exhibits a Toughness Increase Over Deep-Crack Data

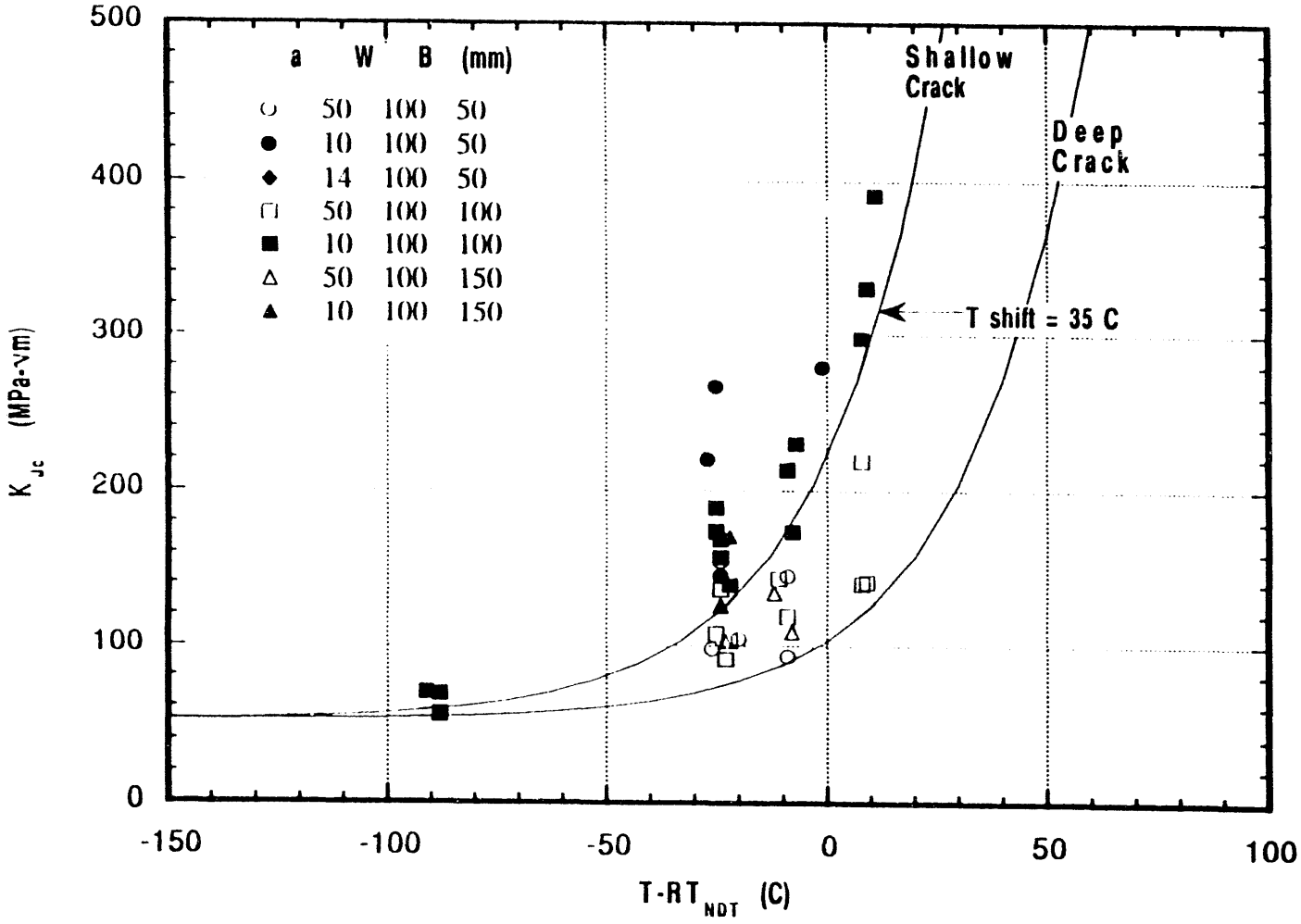

Biaxial Loading Could Reduce the Shallow-Crack Toughness Increase

SENB Data Show an Increase in Fracture Toughness and Data Scatter for Shallow-Crack Specimens Compared to Deep-Crack Specimens

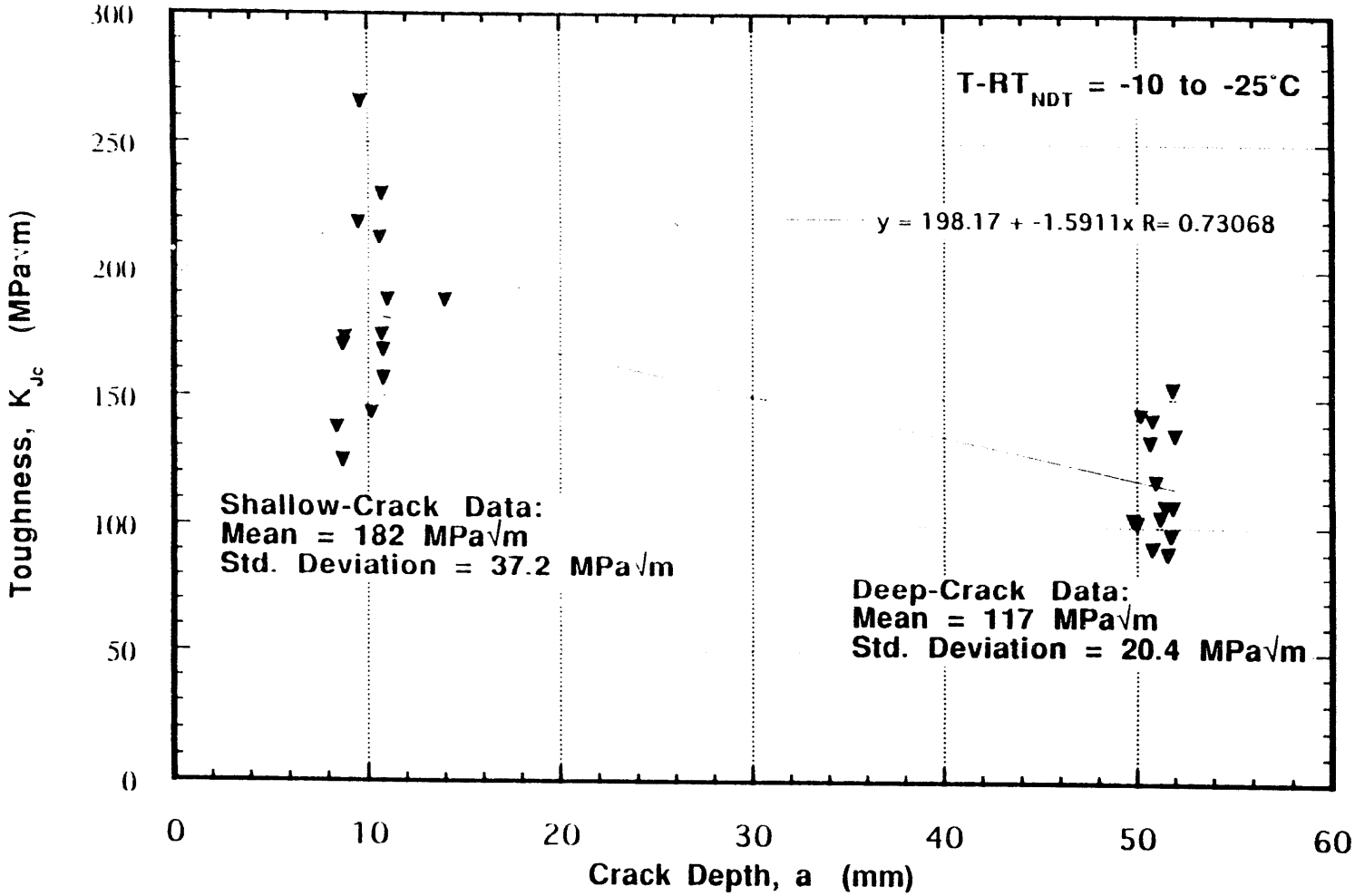

Applications of The Dodds-Anderson Constraint Adjustment Procedure to SENB Data Produce Fracture Toughness Values Independent of Crack Depth

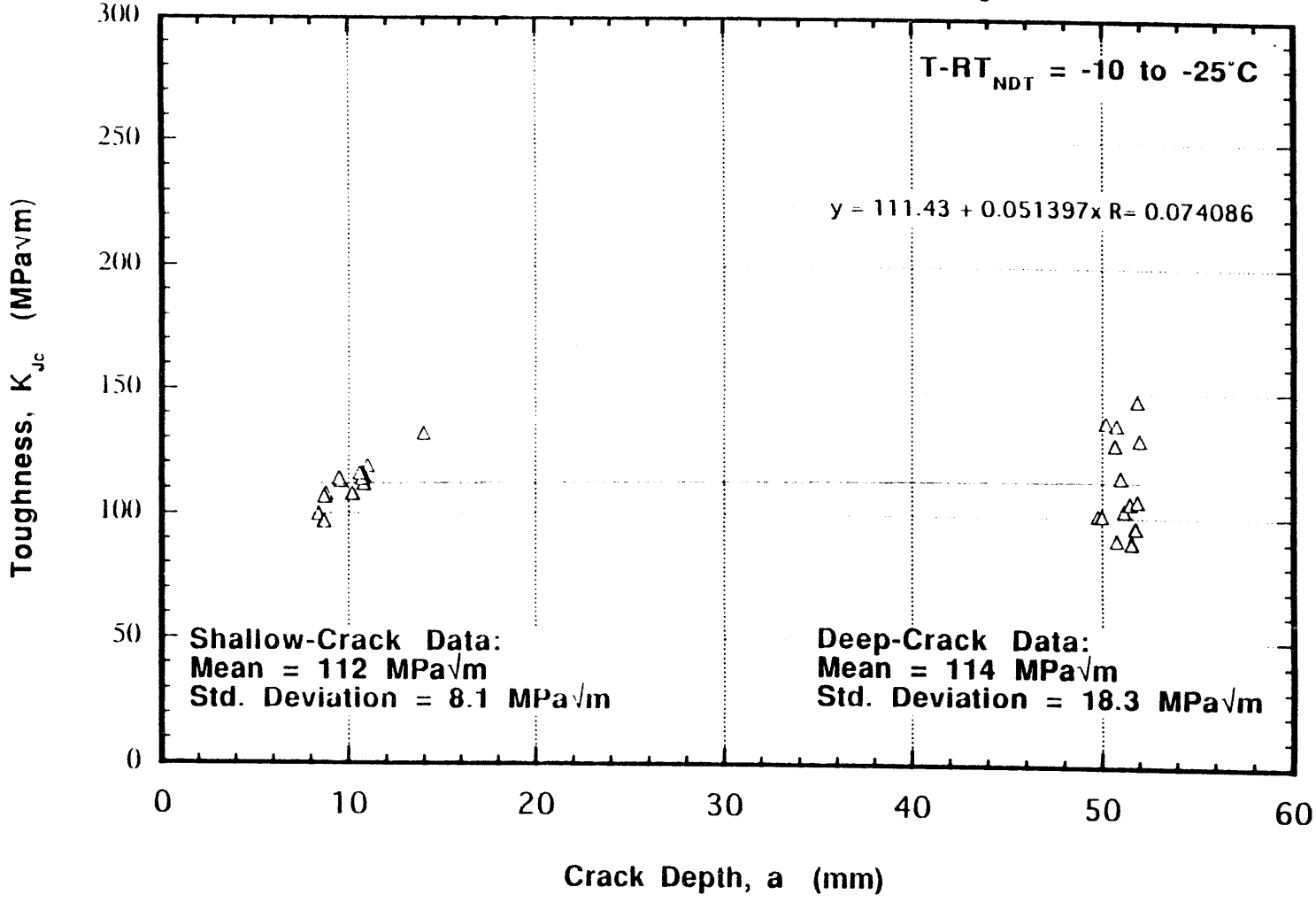

The Shallow-Crack SENB Specimens Exhibit a Q-Stress at Failure of ~ - 0.7, Which Represents a Significant Loss of Constraint

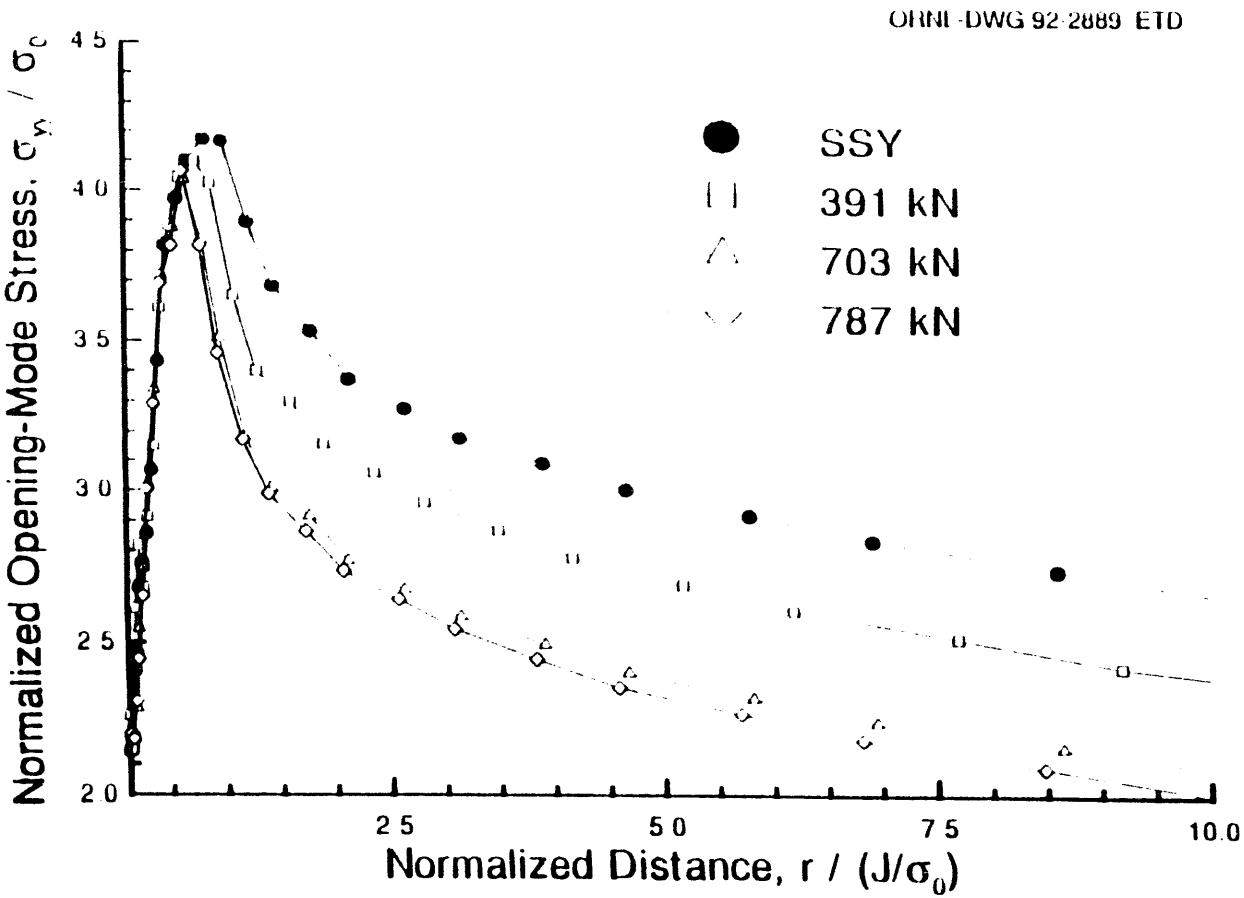

The 100-mm-Deep Cruciform Specimen Can Be Tested Under Either Uniaxial or Biaxial Loading

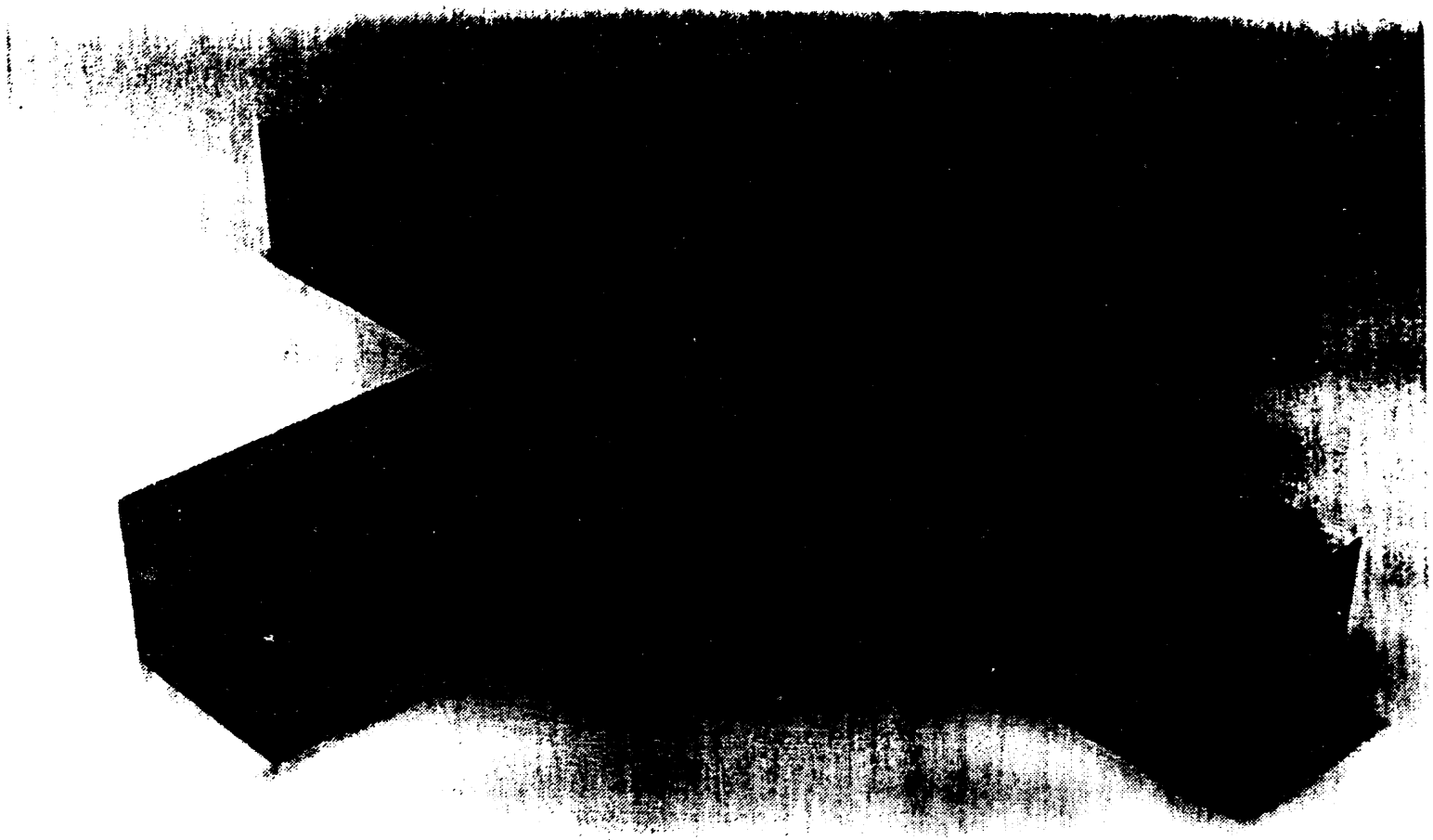

Essential Features of the Infinite-Length Shallow Flaw Geometry and Biaxial PTS Loading are Simulated in the ORNL Biaxial Fracture Toughness Test

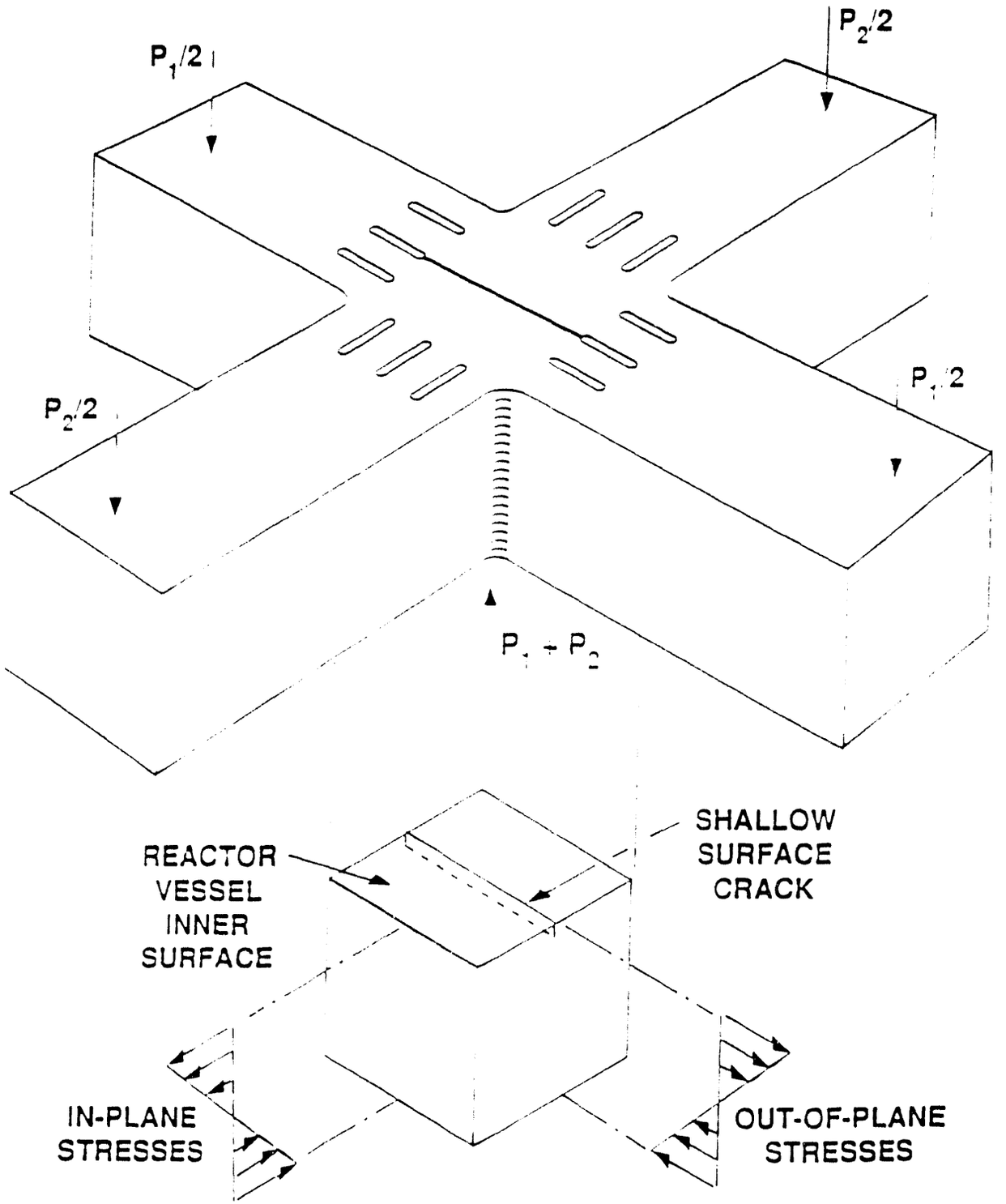

ORNL-DWG 92M-3935A2 ETD

Biaxial, Shallow-Crack Data Tends to Exhibit a Toughness Reduction Compared to Uniaxial, Shallow-Crack Data

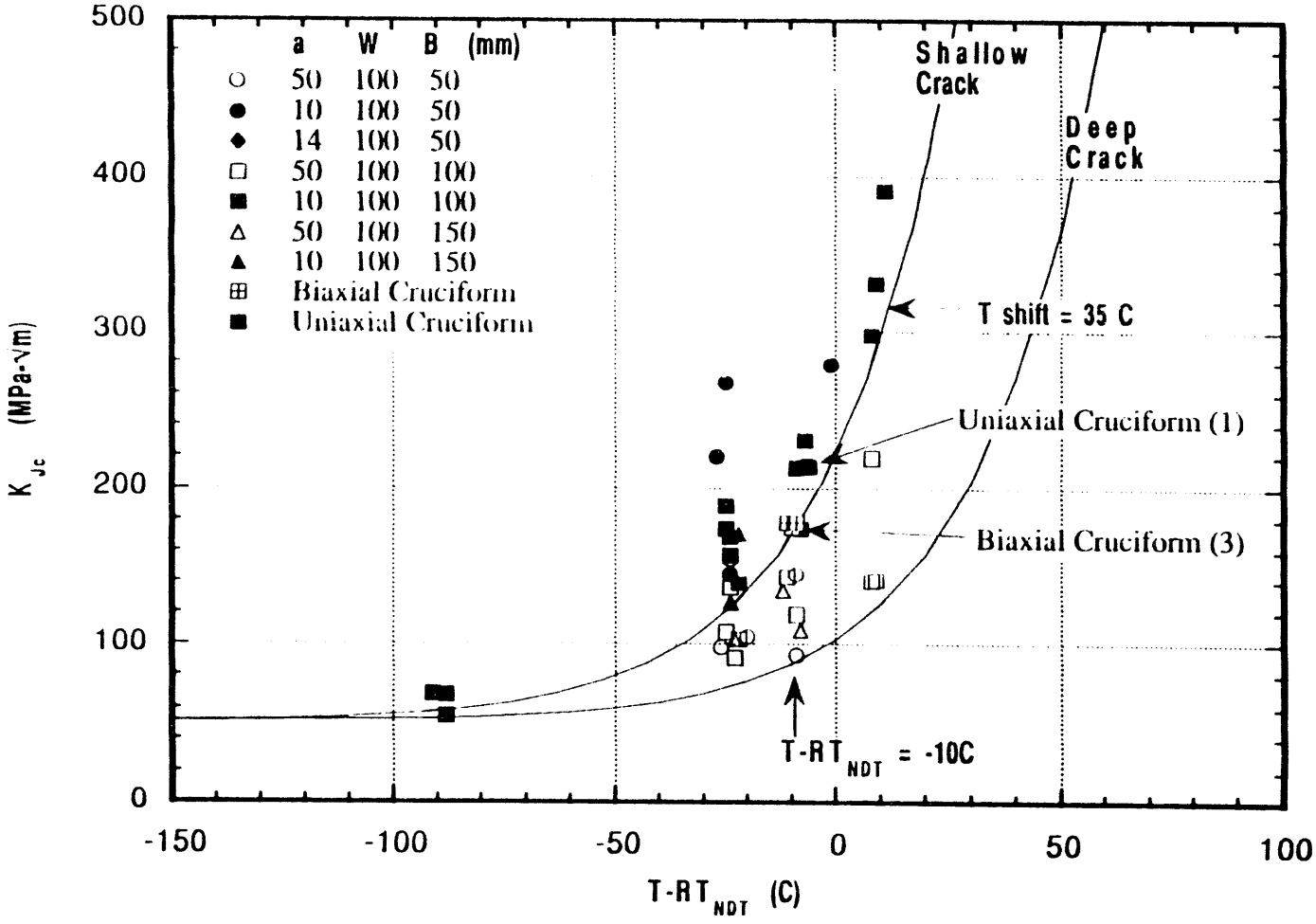

Biaxial Loading (0.6:1) Appears to Cause a 20% Reduction in Fracture Toughness Data Compared to Uniaxial Data

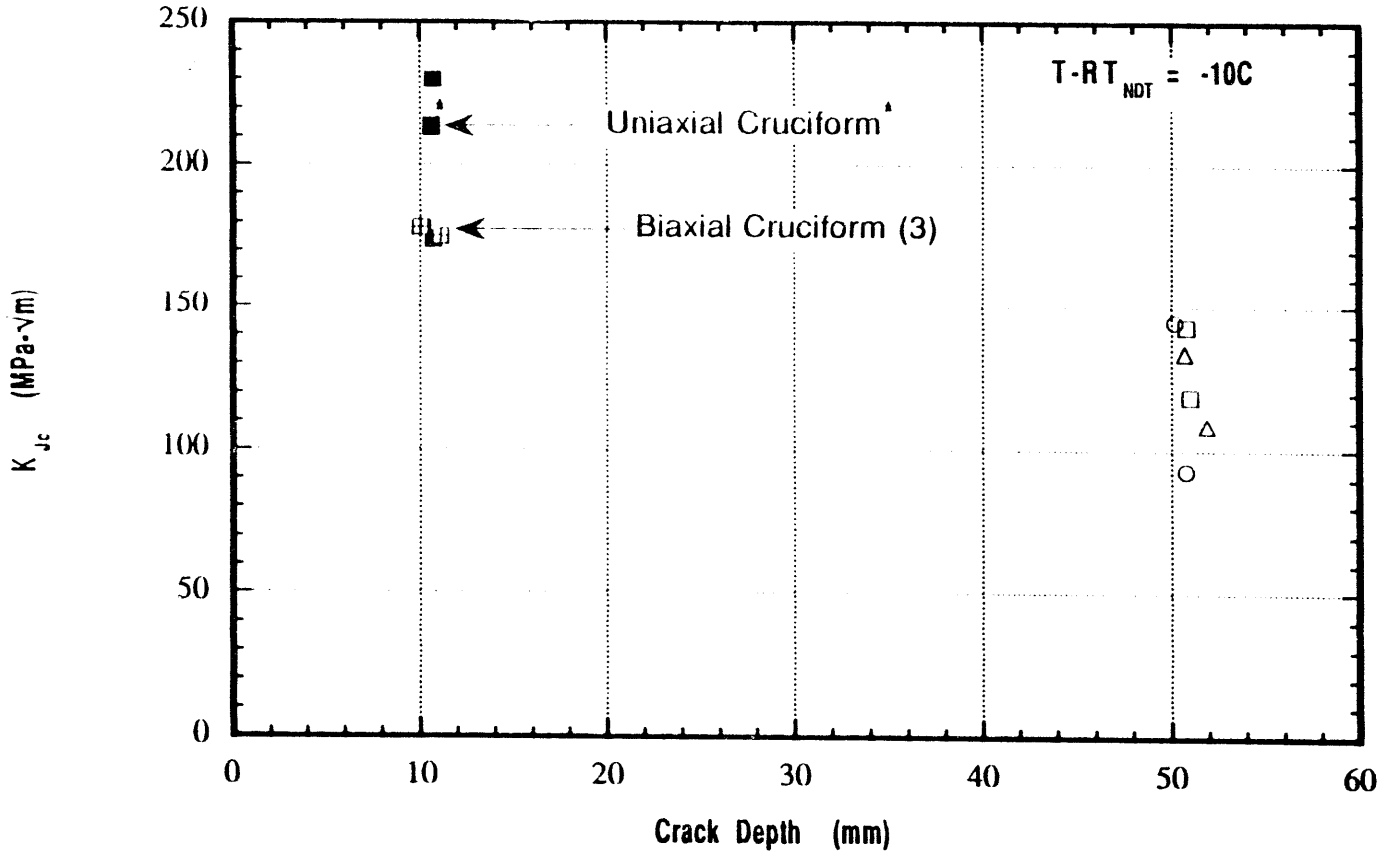

1. Scatter of Biaxial Data Appears Reduced

2. Uniaxial Cruciform Result Is Consistent With Uniaxial SENB Results

Biaxial Loading (0.6:1) Reduces Some But Not All of the Shallow-Crack Toughness Enhancement

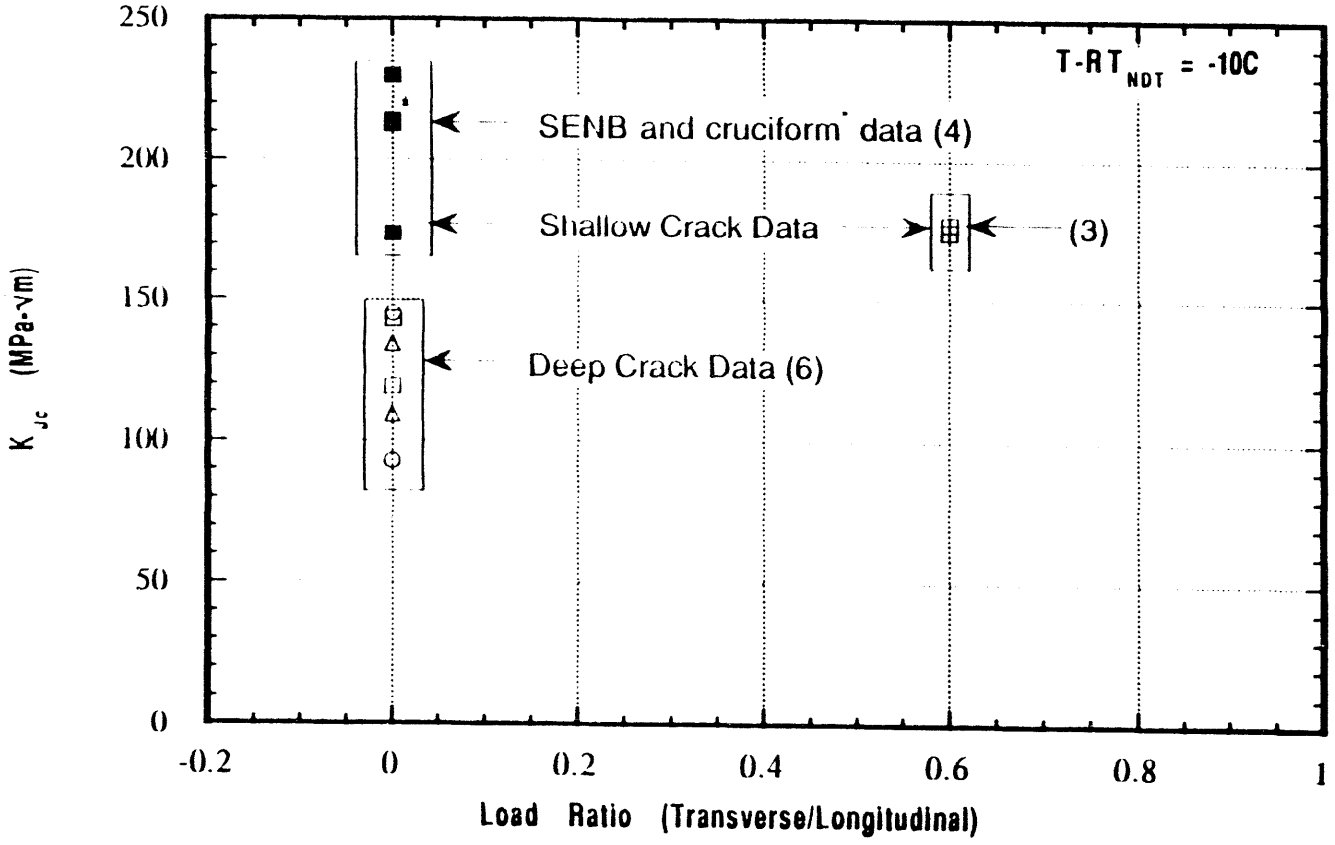

Student's t test indicates three different populations of data

Definition Of Coordinate System And Locations Of Interest For Interpretation Of Finite Element Results From Analysis Of HSST Cruciform Bend Specimen

DIMENSIONS IN mm

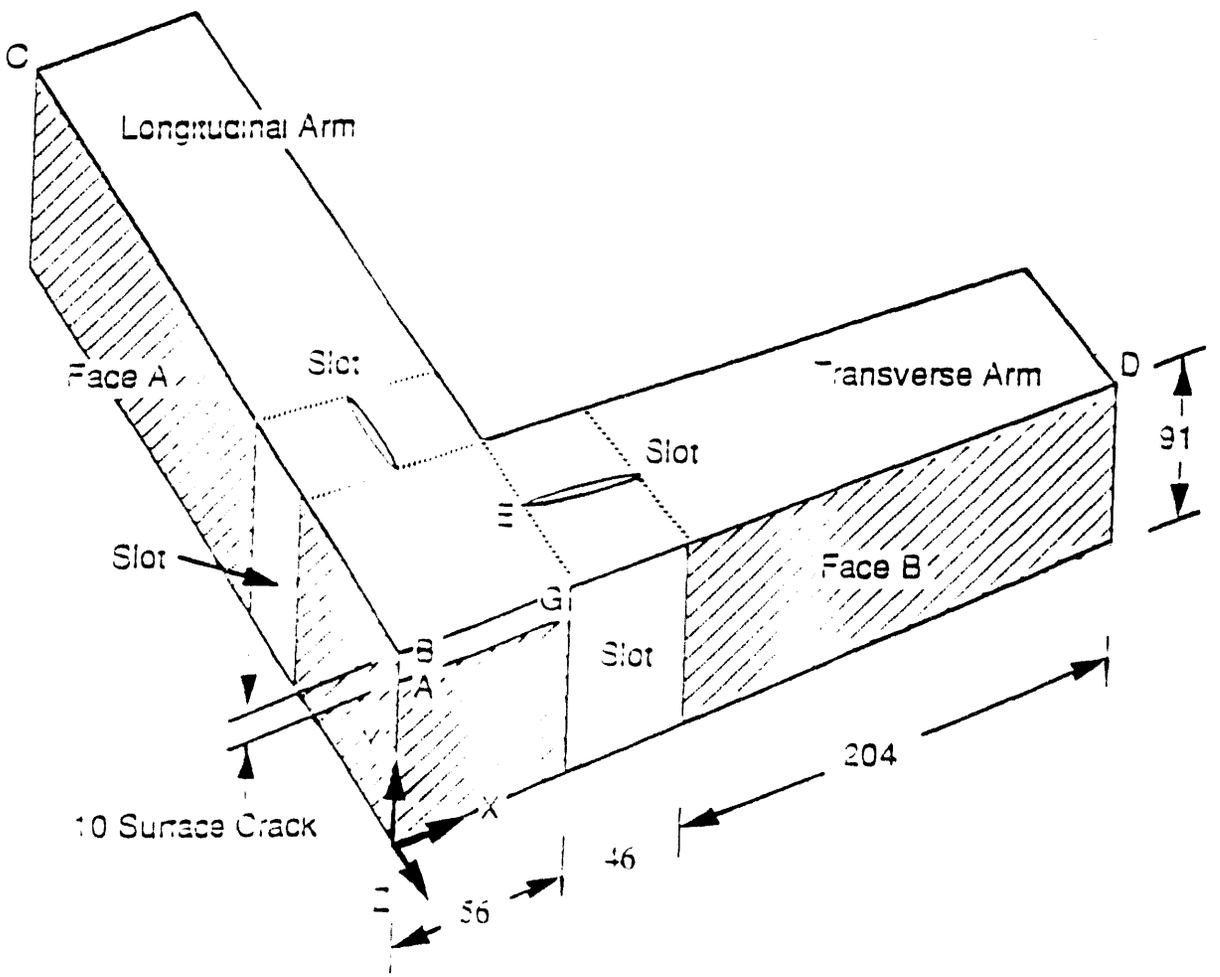

A Cruciform Model Incorporating a Highly Refined Crack-Tip Region is being used for Local Crack-Tip Field Analysis

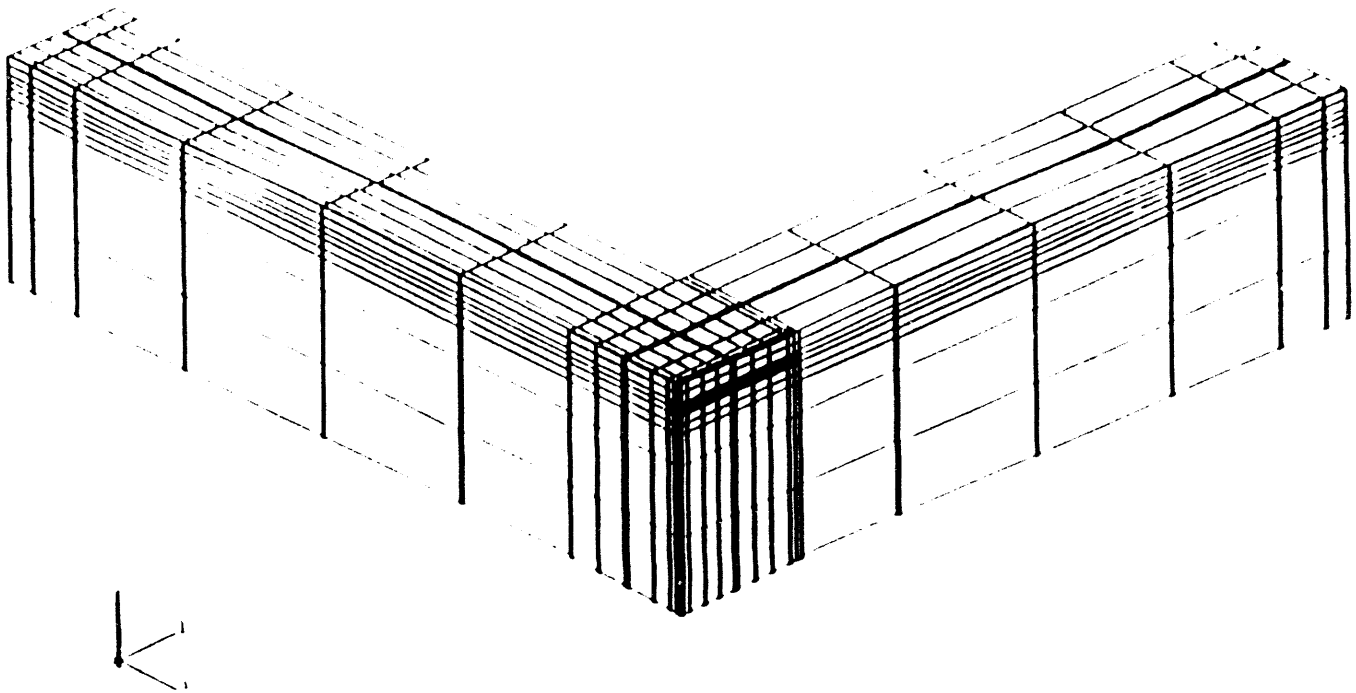

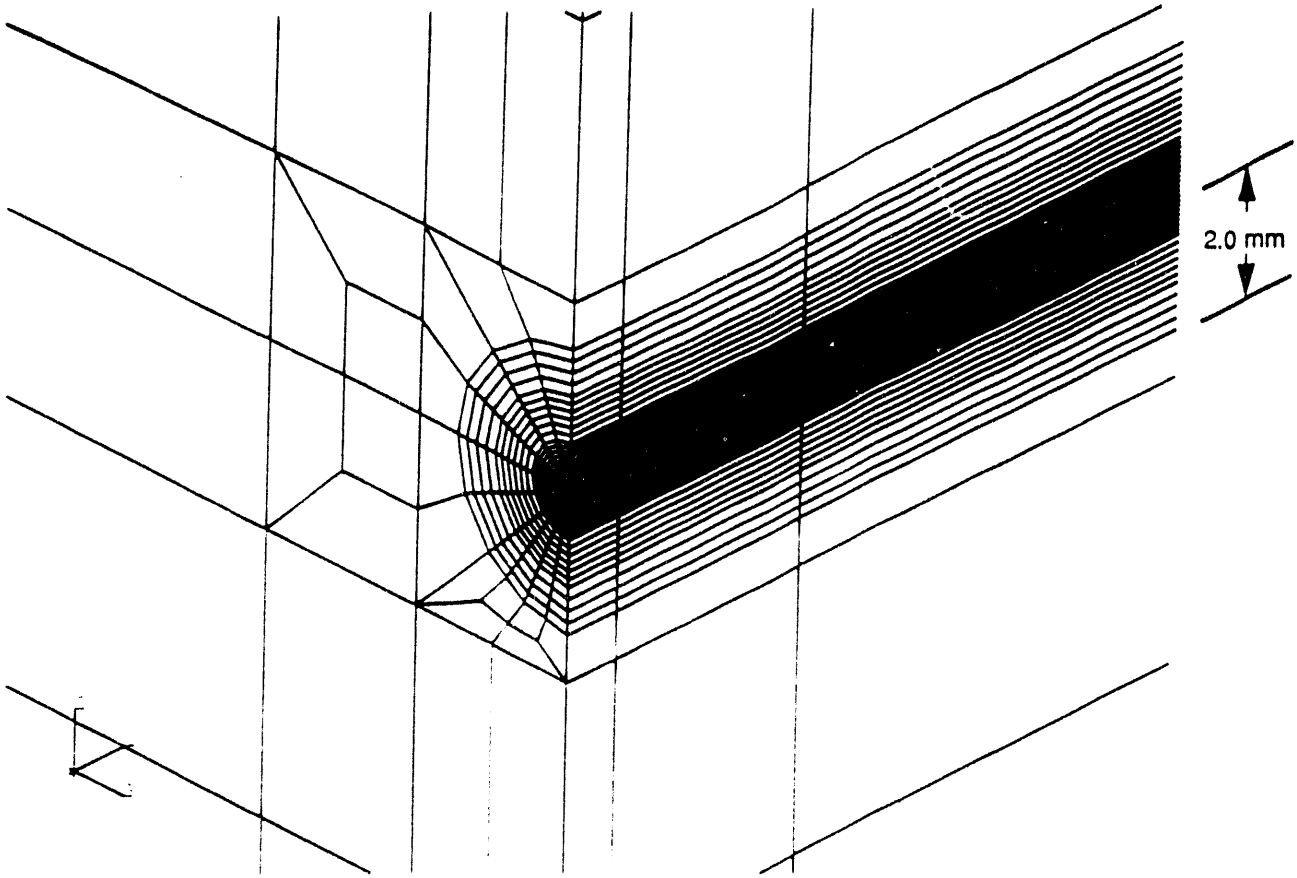
2.0 mm

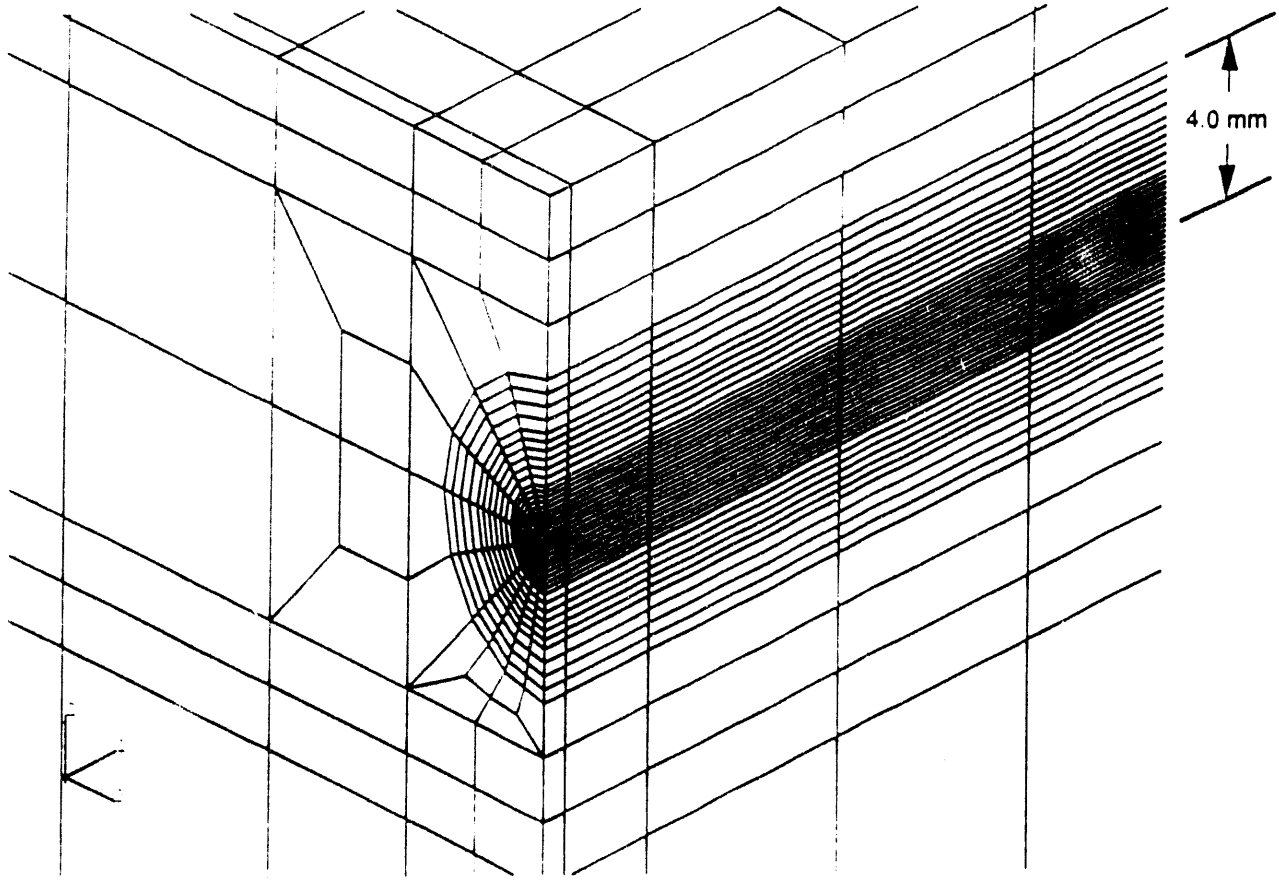
4.0 mm

Two Different Methods Were Used in Applying the Dodds-Anderson Constraint Adjustment Procedure to the Cruciform Data

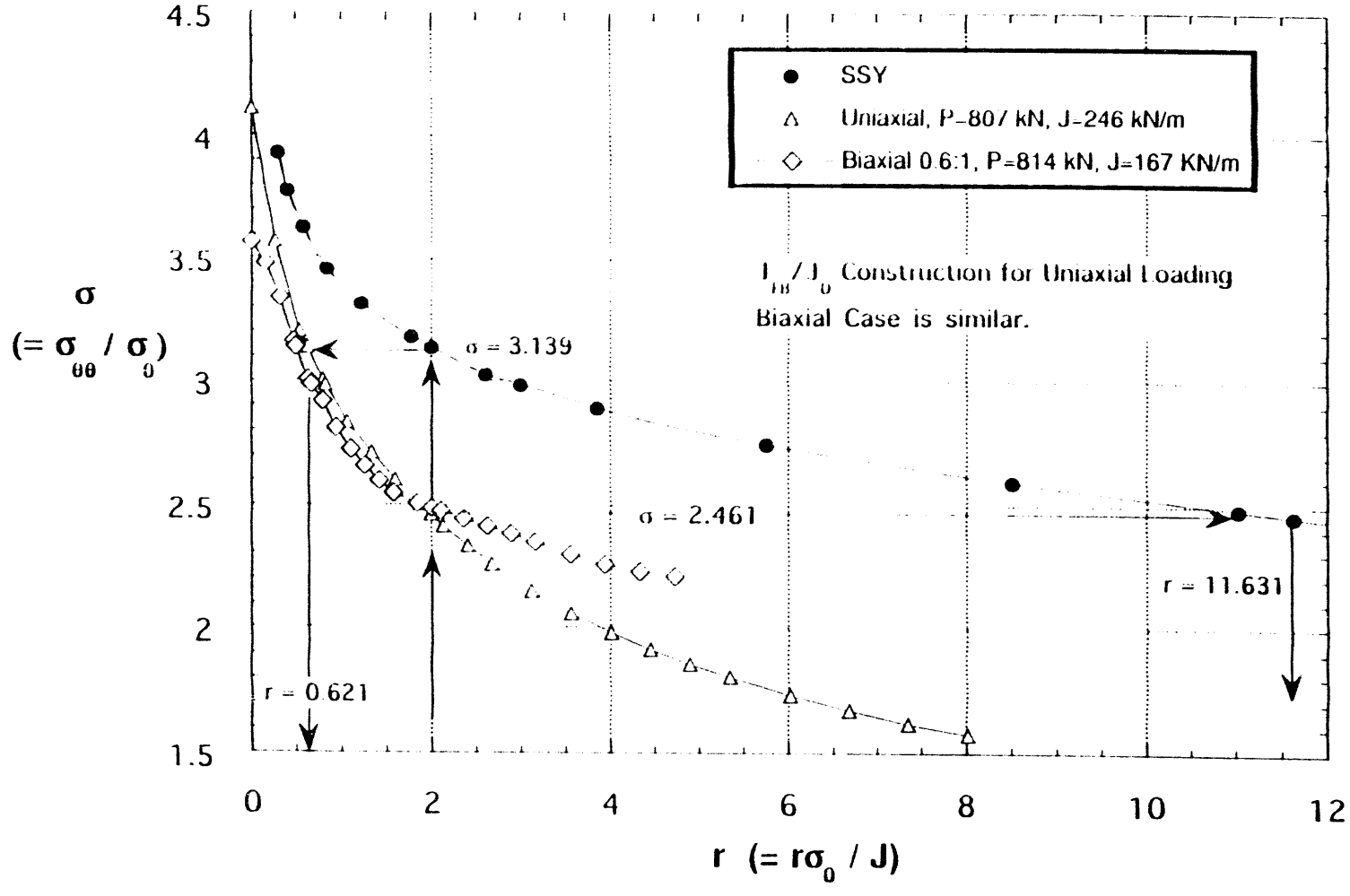

The Constraint Adjustment (or Scaling) Ratios for Biaxial Loading Are ~25% Greater Than Those for Uniaxial Loading; Both Ratios Vary With $\tilde{r}$

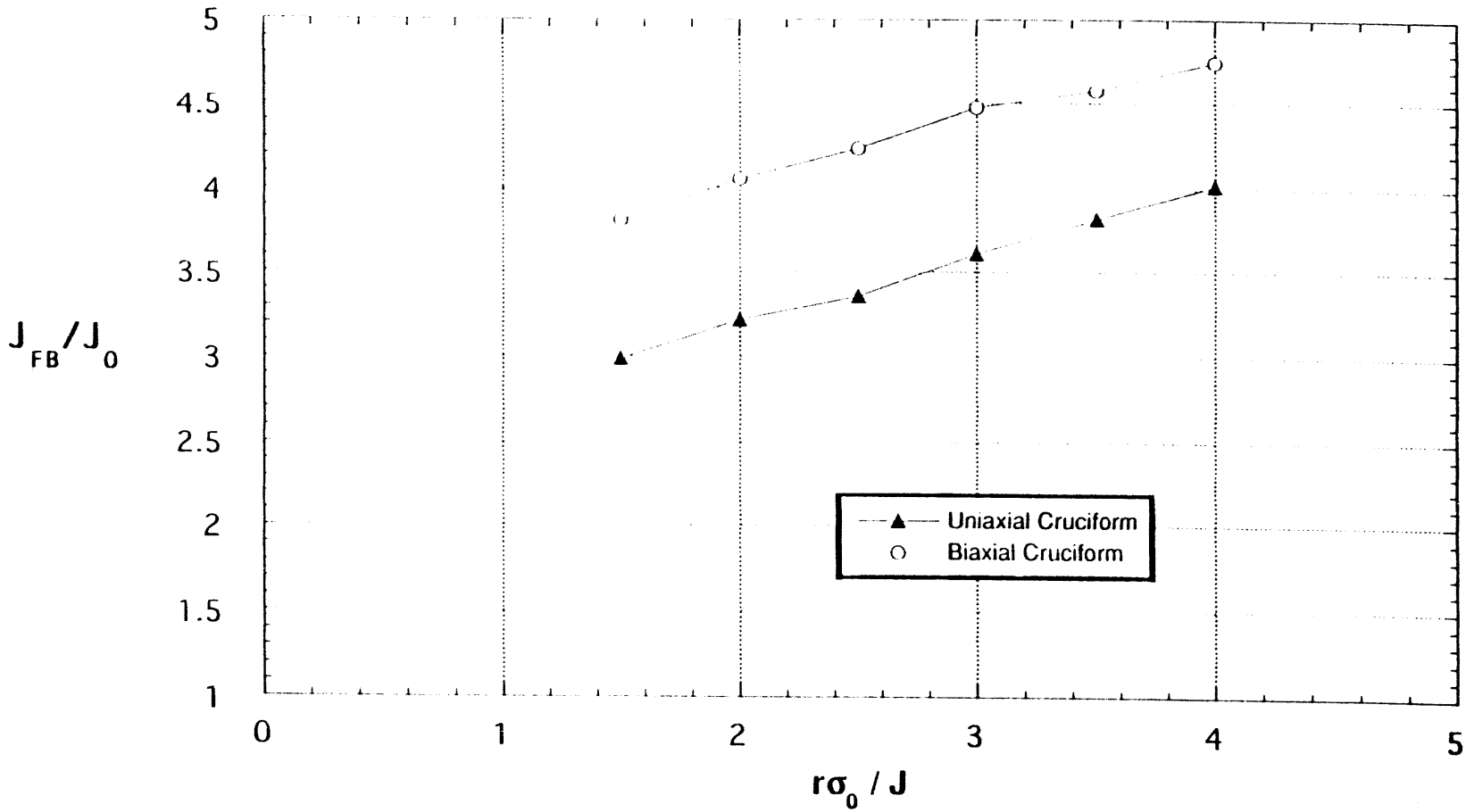

The Cruciform SSY Toughness Values Are Within The Range of SSY Data From SENB Specimens

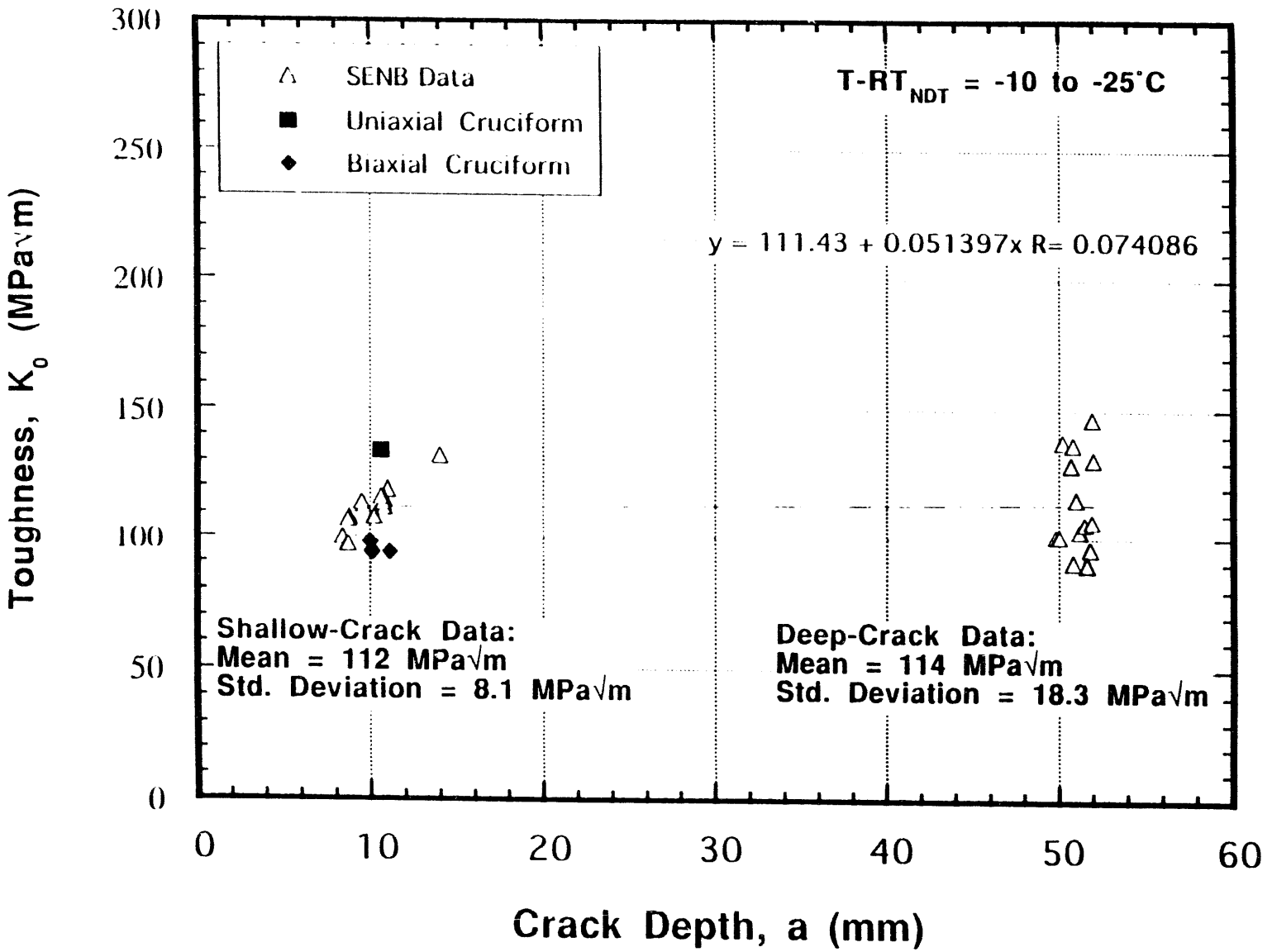

Uniaxial and Biaxial Loading Produce Contrasting Q-Stress Distributions Within the Range $1.5 \leq \tilde{r} \leq 5$

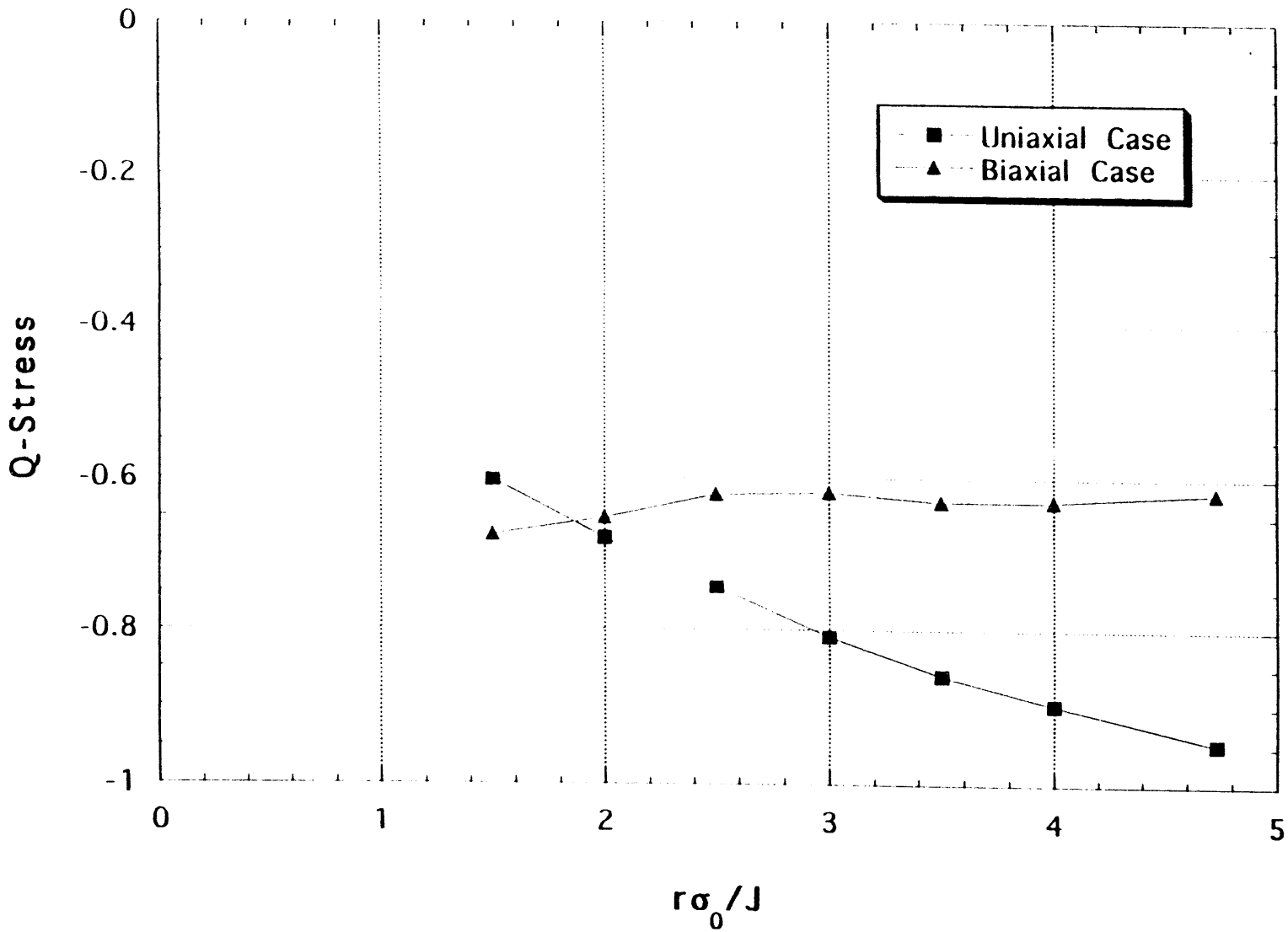

CONCLUSIONS

- Applications of J-Q and Dodds–Anderson methodologies utilized data from specimens providing a contrast in analytical modeling requirements

  – SENB (2-D plane strain)
  – Cruciform beam (fully 3-D)

- Both methodologies were used successfully to interpret experimental data from shallow- and deep-crack SENB specimens.

- Both methodologies showed promising features in applications to cruciform specimens, but also raised several questions concerning interpretation of constraint conditions from near-tip stress fields.

- Unresolved issues identified from analyses require resolution as part of validation process for biaxial loading applications.

END

DATE
FILMED
2/23/94